

This article has been accepted for publication in Monthly Notices of the Royal Astronomical Society ©: 2023 The Authors. Published by Oxford University Press on behalf of the Royal Astronomical Society. All rights reserved.

The interconnection between galaxy mergers, AGN activity, and rapid quenching of star formation in simulated post-merger galaxies

Salvatore Quai ,^{1,2,3*} Shoshannah Byrne-Mamahit ¹, Sara L. Ellison ¹, David R. Patton ⁴ and Maan H. Hani ⁵

¹*Department of Physics and Astronomy, University of Victoria, 3800 Finnerty Rd, Victoria, BC V8P 5C2, Canada*

²*Dipartimento di Fisica e Astronomia ‘Augusto Righi’, Università degli Studi di Bologna, Via Gobetti 93/2, I-40129 Bologna, Italy*

³*INAF-Osservatorio di Astrofisica e Scienze dello Spazio di Bologna, Via Gobetti 93/3, I-40129 Bologna, Italy*

⁴*Department of Physics and Astronomy, Trent University, 1600 West Bank Drive, Peterborough, ON K9L 0G2, Canada*

⁵*Department of Physics and Astronomy, McMaster University Hamilton, ON L8S 4M1, Canada*

Accepted 2022 December 14. Received 2022 December 6; in original form 2022 September 30

ABSTRACT

We investigate the role of galaxy mergers on supermassive black hole (SMBH) accretion and star formation quenching in three state-of-the-art cosmological simulations with contrasting physics models: EAGLE, Illustris, and IllustrisTNG (TNG). We find that recently coalesced ‘post-mergers’ in all three simulations have elevated SMBH accretion rates by factors of ~ 2 – 5 . However, rapid (within 500 Myr of coalescence) quenching of star formation is rare, with incidence rates of 0.4 per cent in Illustris, 4.5 per cent in EAGLE, and 10 per cent in TNG. The rarity of quenching in post-mergers results from substantial gas reservoirs that remain intact after the merger. The post-mergers that do successfully quench tend to be those that had both low pre-merger gas fractions as well as those that experience the largest gas losses. Although rare, the recently quenched fraction of post-mergers is still elevated compared to a control sample of non-mergers by factors of two in TNG and 11 in EAGLE. Conversely, quenching is *rarer* in Illustris post-mergers than in their control. Recent observational results by Ellison et al. have found rapid quenching to be at least 30 times more common in post-mergers, a significantly higher excess than found in any of the simulations. Our results therefore indicate that whilst merger-induced SMBH accretion is a widespread prediction of the simulation, its link to quenching depends sensitively on the physics models, and that none of the subgrid models of the simulations studied here can fully capture the connection between mergers and rapid quenching seen in observations.

Key words: galaxies: evolution – galaxies: general – galaxies: interactions – galaxies: star formation.

1 INTRODUCTION

Mergers are amongst the most catastrophic events that occur in galaxies. Early works with N -body simulations on idealized mergers showed how tidal forces dramatically distort and deform merger remnants (Toomre & Toomre 1972; White 1978; Roos & Norman 1979). Both theory (e.g. Villumsen 1982; Di Matteo et al. 2007; Cox et al. 2008; Lotz et al. 2008; Moreno et al. 2015) and observations (e.g. Hernández-Toledo et al. 2005; Patton et al. 2005; De Propriis et al. 2007; Casteels et al. 2014; Patton et al. 2016) indicate that the ultimate morphological outcome of the interaction is driven by orbital properties and mass ratio of the progenitors, and by physical properties of the involved galaxies.

Furthermore, simulations have long predicted that galaxy mergers induce gravitational instabilities in the interstellar medium (ISM) due to a redistribution of angular momentum, thus driving gas towards the inner part of galaxies (e.g. Hernquist 1989; Barnes & Hernquist 1996; Mihos & Hernquist 1996; Blumenthal & Barnes 2018). Theory predicts that such strong gas inflows from the outer

disc to the inner kpc should induce an enhancement in central star formation rates (e.g. Cox et al. 2008; Di Matteo et al. 2008; Hopkins et al. 2008; Sparre & Springel 2016), and a dilution in central gas-phase metallicity (e.g. Montuori et al. 2010; Torrey et al. 2012; Bustamante et al. 2018). Observational studies of galaxy–galaxy mergers give support to the theoretical framework. Merging galaxies show enhanced SFRs (e.g. Ellison et al. 2008; Li et al. 2008; Patton et al. 2013; Knapen, Cisternas & Querejeta 2015; Cao et al. 2016), and central metallicity dilution (e.g. Ellison et al. 2013b; Grønnow, Finlator & Christensen 2015; Thorp et al. 2019; Bustamante et al. 2020).

Following the pioneering work of Springel et al. (2005b), galaxy formation models generally invoke active galactic nuclei (AGNs) feedback mechanisms to efficiently quench star formation in massive galaxies, especially as a consequence of a merger (e.g. Di Matteo, Springel & Hernquist 2005; Hopkins et al. 2008). Indeed, during galaxy–galaxy interactions, theory predicts that part of the in-falling gas should feed the central supermassive black hole (SMBH), thus leading to rapid black hole growth and triggering AGN feedback with the release of energy (e.g. Lynden-Bell 1969; Cattaneo et al. 2009; Capelo et al. 2015). A fraction of the energy ejected from

* E-mail: salvatore.quai@unibo.it

the AGN feedback, in turn, couples with the surrounding interstellar medium and drives out a significant amount of gas from the galaxy (e.g. Silk & Rees 1998; Murray, Quataert & Thompson 2005; Fabian, Celotti & Erlund 2006; Cattaneo et al. 2009).

However, in the last decade there has been an intense debate in the community about the role of mergers in triggering AGN activity. Many observational studies did not find evidence of merger-driven AGN activity (e.g. Cisternas et al. 2011; Schawinski et al. 2011; Kocevski et al. 2012; Villforth et al. 2014; Hewlett et al. 2017; Shah et al. 2020; Lambrides et al. 2021), while many others have found robust proofs for an AGN excess in interacting galaxies (e.g. Alonso et al. 2007; Ellison et al. 2011; Bessiere et al. 2012; Ellison et al. 2013a; Kocevski et al. 2015; Hewlett et al. 2017; Marian et al. 2020; Pierce et al. 2022). It is possible divergent results arise from different experimental set up, including (not exhaustively) mixed definitions of AGN, mixed low and high redshifts selection, lack of matched controls, AGN fraction in mergers versus excess of mergers amongst AGN, and/or different wavelength range involved (e.g. a larger importance of mergers in mid-IR AGNs than in optically selected ones; Satyapal et al. 2014; Goulding et al. 2018; Ellison et al. 2019; Gao et al. 2020). However, Ellison et al. (2019) ruled out the possibility that the tension could be due to different methodologies, at least for the low redshift infrared selected AGN. Furthermore, outcomes from cosmological simulations suggest that the majority of low-redshift AGN should not reside in recent mergers (Steinborn et al. 2018; McAlpine et al. 2020; Byrne-Mamahit et al. 2022). However, even though most AGNs are not triggered by mergers, mergers can still lead to AGN. For example, in Byrne-Mamahit et al. (2022) we demonstrated that post-mergers from the IllustrisTNG (TNG) simulation (Nelson et al. 2017; Pillepich et al. 2017b; Springel et al. 2017; Marinacci et al. 2018; Naiman et al. 2018) host an excess of AGN and that the majority of post-mergers have above average SMBH accretion rates, consistent with the prediction of enhanced AGN activity. However, there is no consensus about either the physical processes governing feedback mechanisms associated with AGNs (thermal energy, kinetic energy, a combination of the two), nor its extent (range, scales involved, strength). Different models implement different prescriptions for describing AGN feedback and the fraction of energy released, often leading to a dissimilar impact on galaxy evolution (e.g. Schaye et al. 2015; Somerville & Davé 2015; Weinberger et al. 2017). It is therefore important to investigate whether the results of Byrne-Mamahit et al. (2022) are robust to variations in AGN feedback models. The first major goal of this paper is to rigorously compare the AGN-driven merging scenario in three state-of-the-art cosmological simulations: EAGLE (Crain et al. 2015; Schaye et al. 2015; McAlpine et al. 2016), Illustris-1 (Vogelsberger et al. 2014), and TNG100-1.

Beyond the mere triggering of nuclear accretion, theoretical predictions of merger-driven AGN activity have long suggested that galaxy mergers might be the leading mechanism for rapid galaxy quenching (e.g. Di Matteo et al. 2005; Springel, Di Matteo & Hernquist 2005c; Springel 2005; Croton et al. 2006; Hopkins et al. 2008; Somerville et al. 2008). Effective kinetic AGN feedback triggered by gas with low angular momentum which is accreting onto the central SMBH could potentially drive out the gas from the galaxy and heat the circumgalactic medium (CGM), thus halting star formation and hampering the replenishment of the galactic gas supply.

Many previous simulations that linked mergers to AGN activity were able to efficiently remove gas from the galaxy reservoir, leading to a prompt quenching shortly after the coalescence phase (e.g. Springel 2005; Bower et al. 2006; Hopkins et al. 2008; Khalatyan

et al. 2008). Such early works tended to implement very aggressive AGN feedback prescriptions, thus provoking an immediate evacuation of the gas from most post-coalescence galaxies. Recent results also support a pivotal role of mergers to halt star formation. For instance, studies based on the so-called ‘genetic modification approach’ (Roth, Pontzen & Peiris 2016), that are capable of altering the accretion history of a galaxy by generating sets of controlled numerical realizations in a fully cosmological context, have demonstrated a causal connection between mergers and quenching (e.g. Pontzen et al. 2017; Sanchez et al. 2020; Davies, Pontzen & Crain 2022). The genetic approach grants the advantage of controlling the main parameters involved in the galaxy interaction, thus allowing the search for causal connections between the various physical processes involved. However, currently the results are limited to a restricted number of objects covering a small dynamical range of masses, orbits, mass ratios, and other physical properties that might be at play during mergers.

Many other recent works based on the statistical analysis of cosmological hydrodynamical simulations, which include complete samples of mergers covering a realistic range of parameters such as galaxy morphology, gas fraction, and orbital geometry, have instead challenged the merger-driven quenching scenario (e.g. Weinberger et al. 2018; Correa, Schaye & Trayford 2019; Rodríguez Montero et al. 2019; Pathak, Belli & Weinberger 2021; Quai et al. 2021). In Quai et al. (2021), we quantified that only ~ 5 –10 per cent of post-mergers selected from an unbiased TNG300-1 galaxy sample quench as a direct consequence of mergers. In this work, our second major goal is therefore to test whether the lack of merger-driven quenching is ubiquitous in the three aforementioned cosmological simulations and how their different prescriptions for AGN activity reflect upon the outcome of the quenched fraction in the global post-merger population.

A pivotal point that warrants examination is whether or not the merger-driven quenching scenario is in accordance with observational results. Proving a causal connection between mergers and quenching with observations is challenging. Among the known populations of recently quenched galaxies (e.g. Citro et al. 2017; Quai et al. 2018, 2019), the most promising quenched galaxies that can be directly linked to galaxy–galaxy interactions are those known as ‘post-starburst’, also called ‘E+A’ or ‘K+A’ galaxies. Post-starburst galaxies are systems showing spectroscopical evidence of a sharp decline of star formation following an intense star-burst episode that occurred between 0.5 and 1 Gyr ago (e.g. Dressler & Gunn 1983; Couch & Sharples 1987; Wild, Heckman & Charlot 2010; Pawlik et al. 2019; Wild et al. 2020). Morphological studies show that post-starbursts often exhibit morphological disturbance and tidal features (e.g. Oegerle, Hill & Hoessel 1991; Zabludoff et al. 1996; Yang et al. 2008; Pawlik et al. 2018; Sazonova et al. 2021; Wilkinson et al. 2022), all characteristics suggesting a merger-driven quenching scenario. To date, most of the observational studies of the merger-driven quenching scenario have focused on determining the frequency of mergers in various post-starburst populations selected via a plethora of methods, finding contrasting results ranging from small fractions ($\lesssim 10$ per cent; Blake et al. 2004; Setton et al. 2022), intermediate fractions (20 – 40 per cent; Wilkinson et al. 2022), and high fractions (up to 60 per cent; Pracy et al. 2009). However, for the purpose of this paper, we are interested in the complementary question of determining what is the fraction of rapidly quenched galaxies in an unbiased sample of recent post-merger galaxies. Thanks to the first statistically robust large sample of pure recent post-merger galaxies selected by Bickley et al. (2022), Ellison et al. (2022) could recently address the latter question, finding a strong

Table 1. A brief summary of the prescriptions for the models of black hole accretion (i.e. note that the three simulations employ accretion rates proportional to the Bondi–Hoyle–Lyttleton accretion rate; Hoyle & Lyttleton 1940; Bondi & Hoyle 1944; Bondi 1952), and AGN feedback in the simulations EAGLE, Illustris-1, and TNG100-1.

	EAGLE	Illustris-1	TNG100-1
BH accretion	The model uses the angular momentum of the surrounding gas to reduce BH accretion rates in small galaxies.	The accretion rate depends on the gas properties at the location of the BH (susceptible to local stochasticity)	A Kernel-weighted accretion rate over 256 neighbouring cells. The accretion rate correlates with the gas properties in the central regions.
AGN feedback	One-mode: (i) thermal, with a net efficiency 0.015; (ii) the energy is released isotropically.	Two-mode (both thermal): (i) At $f_{\text{Edd}} \geq 0.05$, thermal energy is released with a net coupling efficiency 0.05. (ii) At $f_{\text{Edd}} < 0.05$ thermal energy is released in hot bubbles within a radius of ~ 100 kpc from the BHs.	Two-mode: (i) At high accretion rates, a thermal mode, similar to Illustris. (ii) At low accretion rates, a kinetic mode, with directional injection of momentum into surrounding ISM, oriented in a random direction (isotropic feedback over several events).
Note:	The energy is released following a minimum heating temperature criterion: BHs store feedback energy until a threshold amount. This prevents numerical losses and overcooling.	The ‘hot bubble’ model impacts more on the host halo (M/M_{halo} too high).	Note that TNG low-accretion kinetic mode becomes effective at $M_{\text{BH}} \geq 10^{8.2} M_{\odot}$.

excess of quenching in post-mergers. Quantitatively, Ellison et al. (2022) demonstrated that a rapid truncation of star formation is 30–60 times more probable in post-coalescence galaxies than expected in a control sample of non-interacting galaxies, demonstrating an incommensurable dissimilarity with the quenching excess of Quai et al. (2021). The third major goal of this paper is therefore to compare for the first time observational results of merger triggered quenching (from Ellison et al. 2022) with the predictions from the earlier mentioned cosmological simulations, to gain insights into the interconnection between galaxy mergers and star formation quenching.

The paper is organized as follows: in Section 2, we briefly introduce the cosmological simulations used in this work, as well as the methodology to select post-mergers and a control sample of non-interacting galaxies. In Section 3 we present the results. In detail, in Section 3.1 we quantify the enhancement of AGN activity in star-forming post-merger galaxies; in Section 3.2 we measure the impact of mergers on quenching star-formation; in Section 3.3, we compare the quenching excess in simulated post-mergers with that from observations. Finally, we discuss the results in Section 4, and we summarize our work in Section 5.

2 DATA AND METHODS

Black hole accretion and AGN feedback operate on scales below the simulation resolution, and thus require subgrid prescriptions for modelling the physical processes involved. Distinct cosmological simulations might formulate different sub-grid recipes, responding to (1) appropriate calibrations of the simulations via tuning of physical parameters required to reproduce fundamental observed relation scales, and (2) updated models following a continuous improvement of our knowledge on the physical processes. As mentioned in the Introduction, most of the modern hydrodynamical simulations use AGN feedback to halt star formation in massive galaxies, therefore, the choice of different models for regulating black hole accretion and AGN feedback may have important consequences on the merger-driven quenching scenario we aim to address. We compare the

response of three state-of-the-art cosmological simulations (i.e. EAGLE, Illustris-1, and TNG100-1) to describe the interconnection between merger events, black hole activity, and quenching of star formation. Even though the three simulations span a similar volume (cubes of sides around 100 cMpc), and all of them assume black hole accretion to be proportional to the spherically symmetric Bondi–Hoyle–Lyttleton accretion rate (Hoyle & Lyttleton 1940; Bondi & Hoyle 1944; Bondi 1952), they opt for subtly different physical adjustments and implement distinct AGN feedback models, that might result in a diverse response to galaxy merger events. In this section, we give a brief overview of the simulations we use in this work and their sub-grid models governing black hole activity (see a brief summary of the black hole model prescriptions in Table 1). Readers interested in details about different models for AGN feedback and consequent implications on SMBH properties and galaxy evolution are referred to Habouzit et al. (2021, 2022).

2.1 Cosmological simulations

2.1.1 EAGLE

The ‘Evolution and Assembly of GaLaxies and their Environment’ (EAGLE; Crain et al. 2015; Schaye et al. 2015; McAlpine et al. 2016) is a suite of hydrodynamical cosmological simulations spanning a wide range of numerical resolutions and physical models which are implemented using a bespoke version of the Smoothed Particle Hydrodynamics (SPH) code GADGET-3 (Springel 2005). For this work, we use the largest run denoted Ref-L0100N1504, a cubic periodic volume of $(100 \text{ cMpc})^3$ with dark matter and stellar mass resolutions of $9.7 \times 10^6 M_{\odot}$ and $1.8 \times 10^6 M_{\odot}$, respectively.

The EAGLE public catalogues contain only 29 snapshots at redshift $z < 20$, yielding a temporal resolution that is insufficient to cover the rapid changes a galaxy faces during mergers. We use instead a galaxy catalogue (internal team use) with a much denser time grid, including 201 snapshots at redshift $z < 20$, 65 of which at $z \leq 1$ are useful for this work. The cosmological parameters used in EAGLE are in accordance with Planck Collaboration XVI (2014) which is

given by a matter density $\Omega_{\text{M},0} = 0.307$, baryon density $\Omega_{\text{b},0} = 0.04825$, dark energy density $\Omega_{\Lambda,0} = 0.693$, a Hubble parameter $h = 0.6777$, and $\sigma_8 = 0.8288$.

Star formation is implemented via a sub-grid model described in Schaye & Dalla Vecchia (2008) and based on a pressure-dependent relation that converts gas to stars following the Schmidt–Kennicutt law (Kennicutt 1998).

Following the prescription in Springel, Di Matteo & Hernquist (2005a), black holes are seeded as collision-less sink particles with an initial mass of $1.475 \times 10^5 M_{\odot}$ in the centres of black hole-free dark matter haloes exceeding a threshold mass of $1.475 \times 10^{10} M_{\odot}$. Subsequently, EAGLE black holes can grow either via (1) accretion of surrounding material or (2) black hole mergers. Black hole accretion is regulated following a modified Bondi–Hoyle rate (Bondi & Hoyle 1944) that includes a prescription that takes into account the angular momentum of material nearby a black hole (see Rosas-Guevara et al. 2015, 2016). The inclusion of the angular momentum of surrounding gas allows the material to first settle into an accretion disc, thus reducing black hole accretion rates in small galaxies compared to the original Bondi–Hoyle model. Finally, in EAGLE accretion rates are capped at the Eddington limit, to avoid reaching spuriously high accretion rate values.

EAGLE uses single-mode AGN feedback (Booth & Schaye 2009), where energy is injected thermally into the surrounding ISM, with a fixed efficiency (i.e. a fraction of the accreted gas is stochastically converted in thermal energy and released in the region nearby a black hole with a net efficiency of 0.015), independently from halo mass and accretion rate. The thermal energy is released following a minimum heating temperature criterion, that is when the black hole has accreted enough mass that the equivalent energy released is capable of increasing the temperature of the surrounding gas particles, thus preventing numerical losses and overcooling.

2.1.2 Illustris-1

We identify post-mergers galaxies also in the Illustris cosmological simulation (Vogelsberger et al. 2013, 2014). In this work, we use the flagship Illustris-1 (Nelson et al. 2015) run, that covers a comoving cubic volume of side 106.5 cMpc. Illustris-1 has a dark matter and baryonic mass resolutions of $6.3 \times 10^6 M_{\odot}$ and $1.6 \times 10^6 M_{\odot}$, respectively. The simulation runs from redshift 127 to the present day (50 snapshots at redshift $z \leq 1$) using the AREPO moving-mesh code (Springel 2010; Pakmor et al. 2016). The cosmological parameters used in Illustris-1 are in accordance with WMAP 9 (Hinshaw et al. 2013) which is given by a matter density $\Omega_{\text{M},0} = 0.2726$, baryon density $\Omega_{\text{b},0} = 0.0456$, dark energy density $\Omega_{\Lambda,0} = 0.7274$, and a Hubble parameter $h = 0.704$, and $\sigma_8 = 0.809$.

Star formation is implemented in a sub-grid model following the Springel & Hernquist (2003) formalism. Gas particles exceeding a hydrogen number density of 0.13 cm^{-3} are described by a ‘star-forming’ effective equation of state, and their gas is converted to stars stochastically following the Schmidt–Kennicutt law (Kennicutt 1998) assuming a Chabrier (2003) initial mass function (see Nelson et al. 2015, for further details).

In Illustris-1, black hole seeding follows the prescription in Springel et al. (2005a), where massive haloes exceeding $M_{\text{halo}} = 7.1 \times 10^{10} M_{\odot}$ and devoid of central supermassive black holes are seeded with a black hole of initial mass $M_{\text{BH}} = 1.42 \times 10^5 M_{\odot}$. In Illustris, the accretion rate onto the black hole follows an Eddington-capped Bondi–Hoyle–Lyttleton prescription. The accre-

tion rate scales with the local mass density of the gas particle located at the physical position of the black hole itself. To compensate for the unresolved multiphase ISM (Springel et al. 2005b), that produces a non-physical underdensity in the region surrounding the central black holes, the Illustris model introduces a boost factor that increases the instantaneous accretion rate.

Illustris uses a two-mode thermal AGN feedback, with both modes proportional to the amount of mass accumulated into the central black hole. At high accretion rates (i.e. at Eddington fractions $f_{\text{Edd}} = \dot{M}_{\text{BH}}/\dot{M}_{\text{Edd}} > 0.05$), the AGN deposits thermal energy in the region surrounding the black hole, with a net coupling efficiency of 0.05. Instead, at low accretion rates (i.e. at Eddington fractions $f_{\text{Edd}} < 0.05$), Illustris switches to the kinetic mode AGN feedback. The recipe for the low accretion rate regime should mimic the influence of an AGN radio jet (not resolved in the simulation), with hot bubbles of thermal energy deposited in the CGM within a radius of 100 kpc from the central black hole, coupling to the gas with a net efficiency of 0.35. At high accretion rates, the feedback is implemented as a continuous injection of thermal energy into the ISM, thus subject to numerical losses. Therefore, the AGN quench galaxies exclusively through the low accretion mode.

2.1.3 TNG100-1

The IllustrisTNG (TNG) project includes a suite of large-box magnetohydrodynamical cosmological simulations in a Λ CDM universe which provides a statistically robust sample of galaxies spanning a variety of galaxy properties (e.g. mass, environment, star formation rate). The simulations and physical model are introduced in detail in Marinacci et al. (2018), Naiman et al. (2018), Nelson et al. (2017), Pillepich et al. (2017b), Springel et al. (2017). TNG is the descendant of the Illustris cosmological simulation with an improved physical models and numerical scheme. TNG also introduces a number of additional features to obtain a better agreement with observational results. In this paper, we focus on TNG100-1, the highest resolution run for the intermediate publicly released volume of side 110.7 cMpc. TNG100-1 offers excellent statistics, whilst still guaranteeing adequate numerical resolution. TNG100-1 has a dark matter and stellar mass resolutions of $7.5 \times 10^6 M_{\odot}$ and $1.4 \times 10^6 M_{\odot}$, respectively. The simulation runs from redshift 127 to the present day using the AREPO moving-mesh code (Springel 2010; Pakmor et al. 2016). The cosmological parameters used in TNG are in accordance with Planck Collaboration XIII (2016) which is given by a matter density $\Omega_{\text{M},0} = 0.3089$, baryon density $\Omega_{\text{b},0} = 0.0486$, dark energy density $\Omega_{\Lambda,0} = 0.6911$, and a Hubble parameter $h = 0.6774$.

Star formation occurs in a pressurized, multiphase interstellar medium following the Springel & Hernquist (2003) formalism. Gas particles whose density exceeds a threshold of $\sim 0.1 \text{ cm}^{-3}$ are ‘star-forming’ and their gas is converted to stars stochastically following the Schmidt–Kennicutt law (Kennicutt 1998) assuming a Chabrier (2003) initial mass function (see Nelson et al. 2015; Pillepich et al. 2017a, for further details).

Black holes are seeded with an initial mass of $1.18 \times 10^6 M_{\odot}$ at the centres of the potential wells of haloes exceeding a threshold mass of $7.38 \times 10^{10} M_{\odot}$. Black holes can grow their mass either through (1) accretion following a modify Bondi–Hoyle scheme, or (2) mergers with other black holes. The instantaneous accretion rate in TNG does not depend upon the gas particle at the location of the black hole (as in Illustris). Instead, the rate scales following a kernel-weighted gas density over about 256 neighbouring particles

to reduce the dependence on the local gas mass fluctuations, and it is capped at the Eddington rate.

AGN feedback is directly related to the accretion rate onto the central black holes ($\dot{E} \propto \dot{M}_{\text{BH}} c^2$). At high accretion rates quasar, thermal energy is returned to the black hole's environment, whereas at low accretion rates (i.e. kinetic feedback), energy accumulates until it reaches an energy threshold, then kinetic energy is instantaneously released along a random direction into the gas around the black hole (see Weinberger et al. 2017, for further details). As in Illustris, in TNG the high accretion mode is subject to numerical losses. Therefore, quenching in massive galaxies can be obtained only through the kinetic mode at low accretion rates (e.g. Terrazas et al. 2020). Note that TNG low-accretion kinetic mode becomes effective at $M_{\text{BH}} \geq 10^{8.2} M_{\odot}$.

2.2 Methods

For the purpose of this paper, for each galaxy and for its descendants, we retrieve and use stellar, halo, gas, and black hole masses, as well as instantaneous star formation rates. SMBH accretion rates are calculated by averaging the change in SMBH mass between snapshots over the duration of the snapshot. The mean snapshot intervals are ~ 118 Myr, ~ 156 Myr, and ~ 159 Myr for EAGLE, Illustris-1, and TNG100-1, respectively.

2.3 Star-forming post-mergers

We select and follow the evolution of galaxies from the three simulations' merger trees created using the SUBLINK code (Rodríguez-Gomez et al. 2015). Galaxy mergers are defined as nodes in the SUBLINK merger trees (Rodríguez-Gomez et al. 2015). Namely, we define a post-merger (or PM) in the snapshot immediately after the coalescence phase as the remnant of two interacting galaxies. Following Hani et al. (2020) and Quai et al. (2021), our post-merger sample is restricted to those satisfying the following criteria. First of all, post-mergers must be star-forming when first selected (in order that we can later observe them quenching). In practice, this is implemented by requiring SFRs higher than $-\sigma$ from the star-forming main sequence best fit in the given snapshot (i.e. at fixed redshift). We only follow the evolution of post-mergers at redshift $z \leq 1$ (i.e. in the last ~ 8 – 9 Gyr), in order to avoid the vigorous merger activity at higher redshift that would aggravate issues such as numerical stripping and subhalo switching (Rodríguez-Gomez et al. 2015), and to grant a robust sample of long-term non-interacting galaxies that constitute the pool for selecting a suitable control population. Moreover, we limit the analysis to galaxies more massive than $M_* \geq 10^{10} M_{\odot}$, thus ensuring a complete sample of well-resolved post-mergers with a mass ratio (secondary/primary) larger than 1:10. We then apply a mass ratio cut, excluding mergers with a mass ratio (secondary/primary) $\mu < 0.1$. This criterion is strictly connected with the previous one and prevents the analysis of remnants of mergers with a companion less massive than the reliable mass limit of the simulation.

For Illustris-1 and TNG100-1 post-mergers, we further prevent numerical stripping and subhalo switching issues (Rodríguez-Gomez et al. 2015) by adopting the following procedure to estimate the mass ratio of the merger. We define the mass ratio (μ) as the 'mean' mass ratio value measured over maximum 10 snapshots leading up to coalescence. We exclude the maximum and minimum mass ratios from the mean calculation to remove possible extreme variations which we found to be strongly related to the numerical stripping and subhalo switching effect, respectively. In EAGLE, instead, the mass

ratio μ is from McAlpine et al. (2020) and it is computed when the in-falling galaxy onto the main progenitor had its maximum mass.

Finally, for Illustris-1 and TNG100-1 post-mergers we also apply two additional environmental constraints aimed at avoiding post-mergers that are undergoing further close interactions. Following Patton et al. (2020), we measure r_{sep} as:

$$r_{\text{sep}} = \frac{r}{R_{1/2}^{\text{host}} + R_{1/2}^{\text{comp}}}, \quad (1)$$

where r is the 3D separation between the centres of the host (i.e. post-merger in our case) and its closest neighbour, and $R_{1/2}^{\text{host}}$ and $R_{1/2}^{\text{comp}}$ are the stellar half-mass radii of the post-merger and the closest neighbour, respectively. Patton et al. (2020) showed that TNG100-1 galaxies with $r_{\text{sep}} < 2$ had stronger numerical mass stripping effects, hence we exclude them from the following analysis. The second environmental parameter is r_1 , that is defined in Patton et al. (2020) as the 3D separation to the nearest neighbour with stellar mass above 10 per cent of the mass of the galaxy in question. We exclude post-mergers that have $r_1 < 100$ kpc, whose companion could be already interacting with the post-mergers.

Our selection criteria yield three samples at redshift $z \leq 1$ of 1551, 1082, and 560 star-forming post-mergers for EAGLE, Illustris-1, and TNG100-1, respectively. Despite the fact that the three simulations span similar comoving volumes and use similar cosmology, the number of star-forming post-mergers in TNG100-1 is remarkably smaller than in the other two simulations. Fig. 1 shows the distribution in the main parameters (i.e. redshift, stellar mass, gas fraction (f_{gas} , i.e. the fraction of the total gas over the sum of stellar and gas mass), halo mass, SFR, SMBH mass, mass ratio μ , and N_2) defining the EAGLE, Illustris-1, and TNG100-1 post-merger populations. The different number of TNG100-1's star-forming post-mergers compared to the other two simulations is explained by the difference in the halo and stellar mass distributions. In TNG100-1, indeed, there are only a few star-forming post-mergers with $M_{\text{halo}} > 10^{12.2} M_{\odot}$ and $M_* > 10^{10.5} M_{\odot}$, whilst the rest of TNG100-1 massive post-mergers are passively evolving. The three simulations show significant differences in the black hole mass distributions, with TNG100-1 post-mergers harbouring already massive SMBH with masses around $10^8 M_{\odot}$, whilst Illustris-1 and EAGLE post-mergers show a shallower black hole mass distribution, with EAGLE having a considerable tail of galaxies with black holes less massive than $10^6 M_{\odot}$. Instead, the three simulations show a similar distribution in redshift, local density N_2 (defined in Patton et al. 2016, as the number of neighbours within a radius of 2 Mpc), and mass ratio. About the latter parameter, we note that 50.2 per cent, 52.6 per cent, and 49.6 per cent of EAGLE, Illustris-1, and TNG100-1 post-mergers are minor mergers with mass ratio $\mu < 0.25$ (i.e. 1:4 mergers). We address the impact of mass ratio on quenching star formation in Section 4.1.

2.4 Statistical control sample

We are interested in investigating the link between galaxy mergers, AGN activity, and the quenching of star formation. We quantify the impact of galaxy mergers on the quenching of star-formation using an observational approach that consists of identifying control galaxies that are matched to each post-merger galaxy in redshift, stellar mass, and environment (e.g. Ellison et al. 2013b; Patton et al. 2013). In this section, we describe the steps of generating the control sample.

We implement an adaptation of the matching procedure used in Patton et al. (2016, 2020) to select statistical controls (CTRL) for post-merger galaxies in our sample. For each star-forming post-

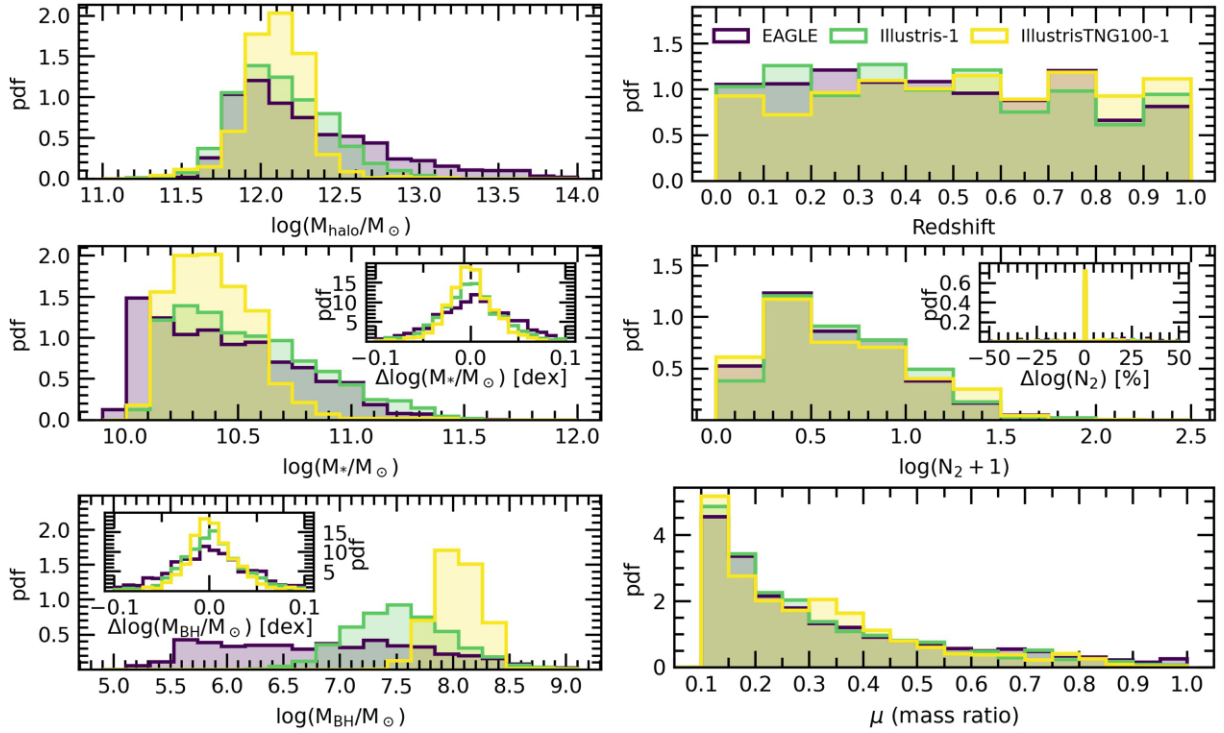


Figure 1. Distribution of the main parameters of star-forming post-mergers selected from the EAGLE (purple), Illustris-1 (green), and TNG100-1 (yellow) simulations. In the left-hand column, we show (from top to bottom) halo mass, stellar mass, and SMBH mass distributions, whilst in the right-hand column, we show (from top to bottom) redshift, the number of neighbours within 2 Mpc (N_2), and mass ratio (μ) distributions. The three insets in the stellar mass, SMBH mass, and N_2 panels represent the distribution of differences (i.e. post-mergers values minus control galaxy values) in the three matched parameters (plus redshift, that is matched de facto as well) following our matching scheme.

merger, we define a star-forming control pool (i.e. non-interacting galaxies with SFR higher than -1σ from the SFMS), at the same redshift (i.e. same snapshot/snapshot), with $M_* \geq 10^{10} M_\odot$, with a relative separation from the nearest neighbour $r_{\text{sep}} \geq 2$, and $r_1 \geq 100$ kpc. We also exclude galaxies that have experienced a merger ($\mu \geq 0.1$) within 2 Gyr. Then, for each post-merger in our sample, we identify the control galaxies that match the post-merger properties as follows:

- (i) $\log(M_*)$ within a tolerance of 0.1 dex.
- (ii) $\log(M_{\text{BH}})$ within a tolerance of 0.1 dex.
- (iii) The environmental parameter N_2 matched within a tolerance of 10 per cent.

If more than one control is found for a given post-merger, we follow the weighting scheme of Patton et al. (2016) to select up to five control galaxies. We then define the post-merger’s *control galaxy* as the single best control galaxy that shares the most number of subsequent snapshots with the post-merger’s descendants whilst maintaining stellar and black hole mass match within a tolerance of 0.2 dex of the descendants’. With our one-control-per-post-merger selection (fiducial matching scheme, in the following), we obtain robust control samples of 1440, 1047, and 548 EAGLE, Illustris-1, and TNG100-1 non-interacting galaxies, respectively. We note that we did not find any control galaxy for 111, 35, and 22 post-mergers in EAGLE, Illustris-1, and TNG100-1, respectively. We exclude these post-mergers without control galaxies from the following analysis. We investigated the bias in the matched post-mergers of the three simulations. We found our matching scheme preferentially failed to find controls in post-mergers with higher stellar and black hole mass. Moreover, a few tens of EAGLE unmatched post-mergers

have intermediate stellar mass with black hole masses that are either in the lower (in most of such cases) or higher envelope of the stellar mass versus black hole mass distribution. We stress that the matching criteria are necessary in order to select an unbiased set of non-interacting control galaxies, therefore, we prioritize the selection of unbiased control samples over the full completeness of the post-merger samples. However, our choice of the maximum tolerances required in our matching criteria returns robust samples of mergers with completeness around 93 per cent in EAGLE and above 96 per cent in Illustris-1 and TNG100-1. Finally, we note that in Section 3.3, we will analyse two matching scheme variations that include a complete sample of post-mergers that are not matched in black hole mass.

The three insets in the right-hand panels of Fig. 1 show the distribution of the differences (i.e. post-mergers values – control galaxy values) in the three matched parameters (note that redshift is matched de facto as well), demonstrating that the differences between the two samples of mergers and controls are well confined within the tolerance limits.

Once the control galaxy sample has been identified, we follow the evolution of the SFR in descendants of post-mergers and controls forward in time through the simulation. For each galaxy, we evaluate the relative level of star formation by calculating, on a logarithmic scale in the SFR– M_* plane, the vertical offset between its SFR and the SFMS (hereafter, ΔSFR). Then, we define galaxies to be quenched when their ΔSFR drops below -0.9 dex (i.e. a deviation of $<-3\sigma$ from the SFMS). Additionally, we quantify the enhancement or deficit of AGN activity in post-mergers as the logarithmic difference between the SMBH accretion rate of each post-merger galaxy and the best matched control (hereafter, $\Delta\dot{M}_{\text{BH}}$), where a positive $\Delta\dot{M}_{\text{BH}}$

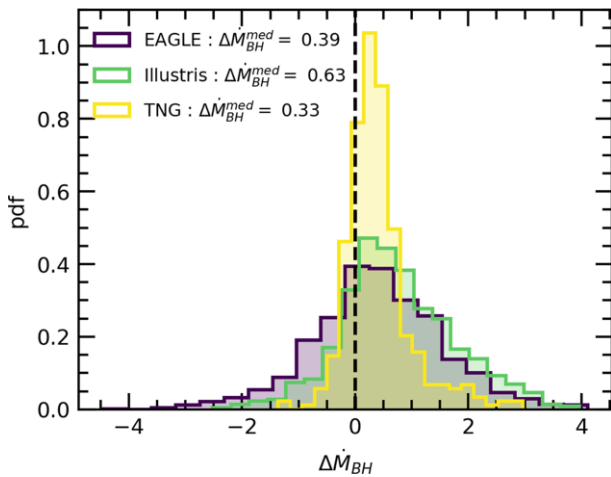


Figure 2. Histogram of the relative offset between the SMBH accretion rates of star forming post-mergers and their best matched controls ($\Delta\dot{M}_{\text{BH}}$). Colours represent different simulations, purple for EAGLE, green for Illustris-1, and yellow for TNG100-1. The figure demonstrates that, on average, the post-mergers from all the three simulations have higher accretion rates than their matched controls. The figure also demonstrates that a significant number (ranging from 20–30 per cent) of post-mergers have similar or lower SMBH accretion rates than controls.

indicates a post-merger SMBH accretion rate $10^{\Delta\dot{M}_{\text{BH}}}$ higher than the control.

3 RESULTS

3.1 Merger-driven AGN activity

The primary goal of this work is to investigate the interconnection between galaxy mergers, AGN activity, and star formation quenching in three state-of-the-art cosmological simulations with publicly available data, i.e. EAGLE, Illustris-1, and TNG100-1. We begin by investigating the enhancement of AGN activity in the star forming post-merger population. Fig. 2 shows the distribution of the logarithmic difference ($\Delta\dot{M}_{\text{BH}}$) between the SMBH accretion rates of post-mergers and controls for each of the three simulations. For the EAGLE simulation, shown in purple, post-mergers have a median accretion rate 2.5 times higher than controls. For the Illustris-1 simulations, shown in green, post-mergers have a median accretion rate 4.3 times higher than controls. Finally, for the TNG100-1 simulation, shown in yellow, post-mergers have a median accretion rate 2.1 times higher than controls, consistent with the results of Byrne-Mamahit et al. (2022) who find post-mergers undergoing high accretion mode feedback (the majority of which are star forming) have accretion rates 1.9 times higher than controls. Therefore, Fig. 2 demonstrates that post-mergers have, on average, higher accretion rates than controls in all three simulations. We find that EAGLE and TNG100-1 have quantitatively similar enhancements in post-mergers. In contrast, Illustris-1 post-mergers have significantly stronger enhancements of accretion rate. The stronger enhancement in Illustris-1 is consistent with the overabundance of efficiently accreting SMBHs in Illustris-1 (Habouzit et al. 2022). In addition to the enhancement in post-mergers, our results demonstrate that enhanced SMBH accretion rates (when compared with controls) are not ubiquitous, and a significant portion (ranging from 20 to 35 per cent) of post-mergers have similar or lower accretion rates

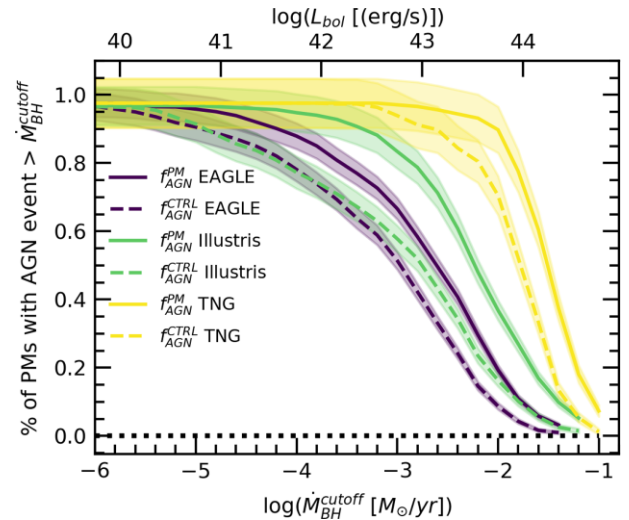


Figure 3. Percentage of star forming post-mergers (solid lines) and controls (dashed lines) which experience an SMBH accretion rate event in excess of $\dot{M}_{\text{BH}}^{\text{cuttoff}}$ within 500 Myr post-coalescence. The top axis shows the equivalent bolometric luminosity, calculated as $0.1\dot{M}_{\text{BH}}c^2$. Colours represent different simulations, purple for EAGLE, green for Illustris-1, and yellow for TNG100-1. The figure demonstrates that instances of high SMBH accretion rates occur more frequently in the post-mergers compared with the controls.

compared with their matched controls. We therefore demonstrate that the majority, but not all, of the star forming post-merger population experiences accretion rates in excess of their matched controls.

We further investigate the incidence of high accretion rate events within the star-forming post-merger population with the following procedure introduced in Byrne-Mamahit et al. (2022). For each post-merger galaxy and its associated control, we follow the post-merger and control forward in time 500 Myr, for intervals of time following the snapshot resolution of the respective simulations. We then determine if, for any snapshot within 500 Myr, the post-merger and/or control has an SMBH accretion rate in excess of a given AGN threshold accretion rate ($\dot{M}_{\text{BH}}^{\text{cuttoff}}$). We note that we only conduct this experiment for post-mergers which can be followed forward in time for 500 Myr. Repeating the experiment for each post-merger in the sample yields the percentage of post-mergers (or controls) that have undergone a high accretion rate event within 500 Myr. Fig. 3 demonstrates the results for EAGLE, Illustris-1, and TNG100-1, where post-mergers are shown as solid lines and controls as dashed lines. The y-axis demonstrates the percentage of post-mergers or controls which undergo an ‘AGN event’, and the x-axis defines the minimum SMBH accretion rate cutoff which defines the ‘AGN event’. Fig. 3 demonstrates that AGN events become more rare with increasing AGN cutoff luminosity. We find that very few (~ 6 per cent) of EAGLE post-mergers have (snapshot averaged) accretion rates above $L_{\text{bol}} \sim 10^{44} \text{ erg s}^{-1}$. Similarly, 17 per cent of Illustris-1 post-mergers have accretion rates above $L_{\text{bol}} \sim 10^{44} \text{ erg s}^{-1}$. In TNG, 60 per cent of post-mergers have $L_{\text{bol}} > 10^{44} \text{ erg s}^{-1}$ in TNG100-1, but there is a rapid decline with no significant amount achieving $L_{\text{bol}} > 10^{45} \text{ erg s}^{-1}$. We note that by design, the simulations limit high accretion rate events, both through the implementation of Eddington limited accretion rates and the transition to effective AGN feedback in TNG at a black hole mass of approximately $10^{8.2} M_{\odot}$. We therefore find highly accreting SMBHs are rare in EAGLE and Illustris-1. However, despite the rarity of the events, they occur more frequently in the post-merger population compared with the

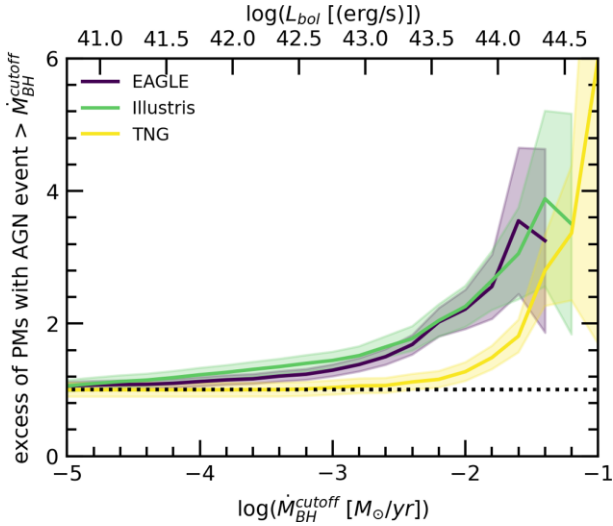


Figure 4. Fractional excess of SMBH accretion rate events (within 500 Myr post-coalescence) in the post-mergers relative to the controls. The top axis shows the equivalent bolometric luminosity, calculated as $0.1\dot{M}_{\text{BH}}c^2$. Colours represent different simulations, purple for EAGLE, green for Illustris-1, and yellow for TNG100-1. The excess is only calculated for values of $\dot{M}_{\text{BH}}^{\text{cuttoff}}$ where there are more than 20 post-merger and non-merger galaxies to ensure statistical robustness. The figure demonstrates that there is an excess of up to 3–4 times more highly accreting SMBHs in the post-merger population.

control population. We note that the average time between snapshots is shortest for EAGLE, which could result in higher average accretion rates, however we find instead that EAGLE produces the fewest galaxies with high SMBH accretion rates. We additionally note that although high accretion rate events are rare in post-mergers, it does not mean that the merging galaxy has not undergone any period of rapid accretion, which may still occur in the pre-merger or ongoing merger phase. In Fig. 4 we show the fractional excess (the ratio of the solid to dashed lines in Fig. 3) as a function of AGN accretion rate. In all three simulations, post-mergers more frequently host highly accreting SMBHs, with an increasing excess as a function of SMBH accretion rate. EAGLE and Illustris-1 demonstrate a peak excess of approximately four, that is four times more post-mergers achieve SMBH accretion rates of $L_{\text{bol}} > 10^{44} \text{ erg s}^{-1}$ compared with controls. Similarly, post-mergers from TNG100-1 achieve a peak excess of approximately five to six, although at higher uncertainty. The fractional excess in TNG100-1 we find here is higher than the excess from Byrne-Mamahit et al. (2022), but is consistent with a stronger enhancement of SMBH accretion rate in the star-forming post-merger sample. Our results are also comparable with McAlpine et al. (2020), who find a maximum AGN excess (comparing post-mergers to a control sample) of approximately two in EAGLE. In fact, it is expected we may find a slightly higher excess over McAlpine et al. (2020), since we are accounting for any AGN event occurring in the snapshots between coalescence and 500 Myr post-coalescence. Overall, Figs 3 and 4 demonstrate in combination that highly accreting SMBH events are rare in the star-forming post-merger population but occur more frequently than in the control population.

3.2 Quenching in post-merger galaxies

Now that we have established the frequency of enhanced SMBH accretion in the post-merger samples, we continue our analysis by

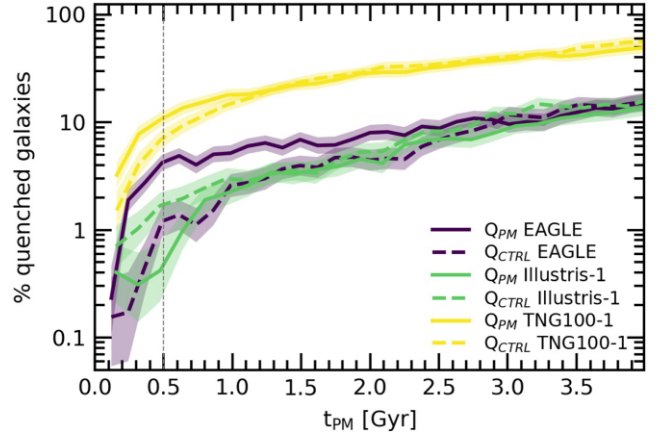


Figure 5. Fraction (expressed in percentage) of post-merger galaxies (Q_{PM} , solid curves) and control galaxies (Q_{CTRL} , dashed curves) that are quenching as a function of time after coalescence (t_{PM}). Colours represent different simulations, purple for EAGLE, green for Illustris-1, and yellow for TNG100-1. The shaded regions represent the 1σ uncertainty on the fraction, estimated following Gehrels (1986). We chose to represent the quenching fraction with a log y-axis scale, to highlight the trend shortly after the merger. The figure demonstrates that all the three simulations have a small fraction of post-merger quenching shortly after coalescence.

studying the impact (or lack thereof) of mergers on star formation quenching. Following Quai et al. (2021), we quantify the effects of mergers using two metrics: (i) the fraction of post-merger descendants with quenched star formation, and (ii) the excess of quenched post-mergers, i.e. the number of quenched post-mergers normalized by the number of quenched controls as a function of time after coalescence. Combined, these two metrics allow us to quantify the absolute rate of quenching in post-mergers, as well as addressing whether quenching is more common in post-mergers than in controls.

In Fig. 5, we show the evolution of the fraction of post-merger galaxies (solid lines) that are quenched as a function of time elapsed since coalescence (t_{PM}). For a qualitative comparison, we show also the behaviour of the control samples (dashed line), that represent the secular incidence of quenching that is expected. The trends of the three simulations are represented with different colours, purple for EAGLE, green for Illustris-1, and yellow for TNG100-1, with the shaded regions enclosing the 1σ uncertainty of the fraction, that we estimate following Gehrels (1986). We note that at $t_{\text{PM}} = 0$, the quenched fraction is 0 because, by construction, we select star-forming post-mergers in our initial sample, hence we begin the analysis from the first snapshot after coalescence.

The quenched fraction of EAGLE’s post-mergers grows faster than their control galaxies in the vicinity of coalescence, though showing only a modest fraction of ~ 4.5 per cent around 500 Myr after coalescence. Later, the increase slows down and levels off to the control quenched fraction (i.e. the expected quenching because of secular evolution) around 3 Gyr after the merger. Looking at the trend from a complementary perspective, the result means that around 90 per cent of EAGLE’s post-mergers that were star-forming during coalescence keep forming stars long after the merger is complete.

Illustris-1 shows very little impact of mergers on quenching star formation, as only 0.4 per cent of them quench within 500 Myr after coalescence (against ~ 1.9 per cent of their control sample in the same period), when mergers are supposed to manifest the maximum effect on the evolution of star formation (e.g. Hani et al. 2019). However, the Illustris-1 trend shows a faster growth in the rate of quenching

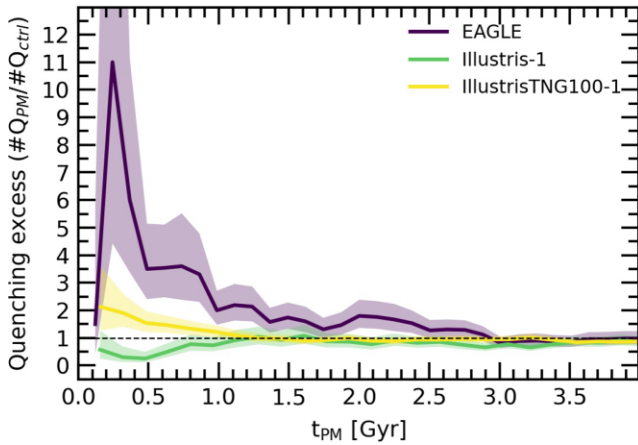


Figure 6. Excess of quenched post-merger galaxies as a function of time after coalescence. The excess is defined as the ratio between the number of quenched post-mergers ($\#Q_{PM}$) and quenched control galaxies ($\#Q_{CTRL}$). Colours represent different simulations, purple for EAGLE, green for Illustris-1, and yellow for TNG100-1. The shaded contours represent the 1σ uncertainty, which is quantified following Gehrels (1986). The horizontal dashed black line represents the same number of quenched post-mergers and controls. The figure indicates that EAGLE shows the largest excess of quenched post-mergers amongst those analysed in this work, with a factor of around 11 times more quenched galaxies than expected from the non-interacting population. Conversely, Illustris-1 shows a deficit of quenching in post-merger galaxies. Finally, TNG100-1 shows an excess of quenched post-mergers, qualitatively and quantitatively comparable with that in Q21.

than EAGLE, thus catching up with the control sample trend around 1 Gyr after the merger, and reaching a quenched fraction ~ 10 per cent 4 Gyr after the merger.

In TNG100-1, we find the largest quenched fraction compared to the other simulations, although reaching only around 10 per cent within 500 Myr after the merger, and levelling off with the control sample trend shortly after 1 Gyr after coalescence. The difference in the quenched fraction trend between TNG100-1 and the other two simulations can be better understood by focusing only on the control sample behaviour. We find that EAGLE and Illustris-1 control samples show a quantitatively similar trend for the entire period analysed, whilst the trend of the TNG100-1 control sample is systematically above, thus suggesting that the main distinction can be ascribed to both a different star formation/quenching regulation in the simulation models (e.g. Donnari et al. 2019) and to our selection of TNG100-1 galaxies that already have massive black holes about to enter (or already have entered) into the effective kinetic mode regime (i.e. $M_{BH} > 10^{8.2} M_{\odot}$, see Fig. 1, and Terrazas et al. 2020). Hence the controls quench just as readily as the merging galaxies.

Fig. 6 shows the quenching excess that quantifies the relative tendency of mergers to experience quenching compared to secular processes which are accounted for in the controls. The layout is the same as in Fig. 5, and the uncertainties are from the binomial statistic (Gehrels 1986). We find that EAGLE (represented in purple) shows the largest excess among the analysed simulations, with a maximum of 11 times more quenched post-mergers than expected in a control sample around 250 Myr after coalescence. Then, the excess decreases steadily until ~ 3 Gyr after the merger, when quenching in post-mergers becomes statistically indistinguishable from that of the control sample. TNG100-1 (shown in yellow) also shows an enhanced quenched fraction, but at a somewhat lower level (factor of two) than in EAGLE. Moreover, the excess vanishes more

quickly than in EAGLE, with the number of quenched post-mergers compatible with that expected from secular evolution beyond 1.2 Gyr after coalescence. Illustris-1 (represented in green), surprisingly shows a deficit, with quenching happening in post-merger galaxies at half the rate expected in controls. The presence of a deficit in quenched post-mergers means that in Illustris-1 mergers are actually halting, or slowing down, the quenching process. The effect of reducing the frequency of quenching is temporary, and the deficit disappears around 1 Gyr after the merger, when the number of post-mergers and controls is statistically equal.

3.3 Comparing post-merger quenched fractions with observations

The picture that arises from our analysis in the previous sections is that mergers in state-of-the-art cosmological simulations may trigger AGN, however, quenching occurs in only a small fraction of merging systems. Although we find a small fraction of promptly quenched galaxies (Fig. 5), none the less there is an excess of quenched post-mergers compared with control galaxies in EAGLE and TNG100-1 (Fig. 6), thus suggesting that mergers in these simulations could contribute to quenching star formation. We stress that our experiment proves how contemporary subgrid models affect the evolution of quenching in simulated merger remnants (see Section 2, and Quai et al. 2021). However, to obtain more accurate and reliable conclusions that can be generalized to the actual Universe, we need to put our results into perspective with robust observational results.

In the Introduction, we mentioned that ‘post-starburst’ galaxies are a useful population for identifying rapid and recent quenching. Briefly, post-starbursts are commonly identified by their optical spectra dominated by an overabundance of A and F types stars (with a lifetime around 1 Gyr), and a lack of spectral features of shorter lived massive O and B types stars, indicating a recent starburst episode followed by a sharp truncation of star formation (e.g. Dressler & Gunn 1983; Couch & Sharples 1987). Post-starbursts could therefore represent the optimal population to causally connect mergers and quenching.

In the literature, however, most studies focus on the fraction of mergers in the post-starburst population, finding values ranging from 10 to 60 per cent (e.g. Blake et al. 2004; Pracy et al. 2009; Setton et al. 2022; Wilkinson et al. 2022). Wilkinson et al. (2022) showed that the post-starburst merger fraction is strongly susceptible to the choice of merger identification metrics and post-starburst selection criteria. Wilkinson et al. (2022) also demonstrated that only ~ 30 per cent of recent mergers in simulations can be recovered using the typical morphology metrics. Therefore, it cannot be excluded that a larger fraction of post-starbursts could have recently undergone a merger. Nevertheless, even in an extreme scenario where nearly all post-starburst galaxies would be post-mergers, it would not answer the complementary question of whether mergers systematically lead to promptly quenched star formation.

Recently, Ellison et al. (2022) analysed a robust and highly pure sample of ~ 700 post-mergers identified by Bickley et al. (2022), the largest pure catalogue to date, allowing them to statistically tackle the frequency of post-starburst galaxies in recent mergers. Applying two different selection methods for detecting post-starbursts, i.e. the ‘E+A’ and the ‘Principal Component Analysis’ (PCA),¹ Ellison et al.

¹The PCA selects galaxies with a relative excess of Balmer absorption lines, thus indicating spectra dominated by A and F types stars, but the method includes also galaxies that show emission lines that might originate from a

(2022) found, respectively, a frequency of 6 and 20 per cent of post-starbursts in the post-merger population. Compared with a control sample of non-mergers, these post-starburst fractions represent a factor 30–60 enhancement, demonstrating that mergers can lead to quenching.

However, Ellison et al. (2022) stress that these observational fractions of post-starbursts in post-mergers are lower limits of the actual quenching fraction for the following reasons. First of all, to pass through the post-starburst phase, a galaxy has to first experience an enhanced star formation phase. However, we know from observations that the majority of post-mergers in the local Universe show a relatively modest enhancement in star formation (e.g. Ellison et al. 2013b; Knapen et al. 2015). Therefore, many post-mergers could quench as a direct consequence of the interaction without passing through the post-starburst phase. A second critical point concerns the different time-scales at play. Galaxy merger features (e.g. morphology disturbance, shells, tidal features, star formation enhancement) tend to vanish on the order of 200–500 Myr after coalescence (e.g. Mihos 1995; Lotz et al. 2008; Hani et al. 2019; Bottrell et al. 2022). The post-starburst phase, instead, arises typically 0.5–1 Gyr after the burst of star formation (Wild et al. 2020). Therefore, many post-mergers might be prematurely observed before the onset of the post-starburst phase. The chance to observe a post-starburst phase in post-merger galaxies scales with a restricted combination of orbital properties, mass ratio, and underlying properties of the galaxies themselves. Mergers with prograde orbits, high mass ratio, and high initial gas mass are able to induce stronger and longer lasting morphology disturbance and quenching (e.g. Bekki et al. 2005; Di Matteo et al. 2007; Lotz et al. 2008; Wild et al. 2009; Moreno et al. 2015; Pawlik et al. 2018; Zheng et al. 2020). Indeed, Ellison et al. (2022) note an enhanced post-starburst fraction in more asymmetric mergers.

In Section 3.2, we measured the fraction of quenched galaxies in the post-merger populations of the three analysed cosmological simulations. We cannot however directly compare our quenched fractions to those of Ellison et al. (2022) because we define the fraction to be the ratio between the number of quenched post-mergers over the number of total post-mergers selected, which by construction belong to the sub-group of star-forming post-mergers at coalescence.

In order to compare with Ellison et al. (2022), we now quote the global quenched fraction, i.e. the number of star-forming post-mergers that quench relative to the total sample of post-mergers which include both the star-forming and non-star-forming populations. Fig. 7 shows the global quenched fraction (top panel) and the quenching excess (bottom panel) within 500 Myr after coalescence of the samples obtained with our fiducial matching selection (see Section 2.4), in comparison to observational results from Ellison et al. (2022). Fig. 7 shows that the quenched fractions measured in the three analysed simulations are below the lower limits of the observational values (both E+A and PCA selection), and significantly below the observational quenching excess values. Only EAGLE’s quenching excess is barely compatible (within errors) with the excess measured with the conservative E+A selection. However, none of the simulations show quenched fraction and quenching excess compatible with the results from the PCA selection.

We test whether the incompatibility between simulations and observational constraints is due to differences in the matching selection criteria. Although the control sample is not used for

non-star-forming source (Wild et al. 2007), which would be instead removed in the E+A selection (e.g. Zabludoff et al. 1996; Goto 2005).

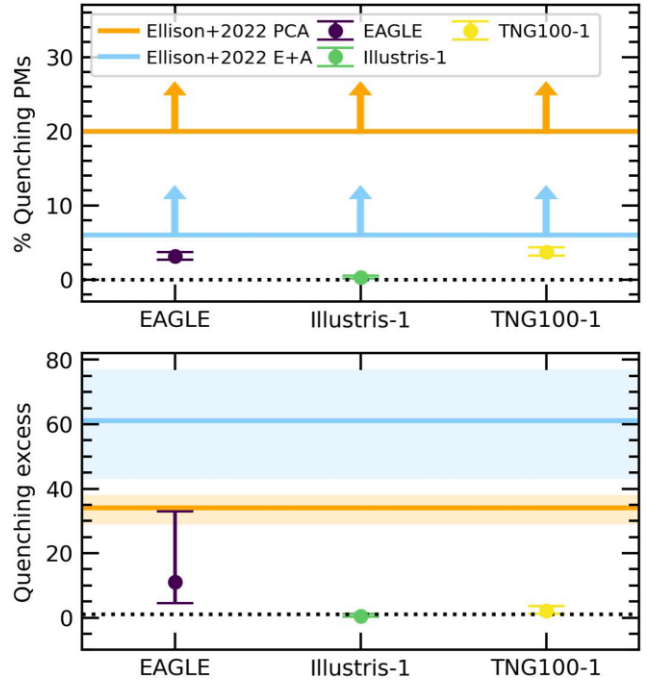


Figure 7. Top: comparison of the global quenched fraction in simulated post-mergers with the post-starburst fraction in mergers from observations in Ellison et al. (2022) (the arrows indicate that values are lower limits, the light blue line represents observed post-starbursts in mergers selected using a classical E+A method, whereas the orange line is for post-starbursts in mergers selected applying a PCA approach). The three symbols and errorbars represent the quenched fraction within 500 Myr from coalescence of, from left to right, EAGLE (purple), Illustris-1 (green), and TNG100-1 (yellow). Bottom: comparison of the quenching excess in simulations with observations. The layout is the same as in the top panel. The figure demonstrates that cosmological simulations like the ones analysed in this paper cannot quantitatively reproduce observational constraints of the impact of mergers on quenching star formation.

measuring the quenched fraction, a different set of matching criteria can modify the completeness of the post-merger sample, because post-mergers that do not have a control are excluded from the analysis. In Ellison et al. (2022) each post-merger is matched to the best non-interacting control galaxy in redshift and stellar mass. Here, we perform two variations of our fiducial matching scheme (see Section 2.4), changing our criteria one step at a time to get closer to the observational control selection. For each variation, we take the maximum quenched fraction within 500 Myr after coalescence, in order to focus on the stage of the merger sequence where it is highest the probability to observationally select galaxies with both post-merger and post-starburst features. This experiment helps us to both compare the simulated and observed merger quenched fraction, and to measure the impact of the matching scheme on our results. The fiducial and the two variation schemes are summarized in the following:

- (i) *Fiducial*. For each star-forming post-merger, we select the best star-forming non-interacting galaxy that is matched in redshift, stellar mass, black hole mass, and environment. See Section 2.4 for details.
- (ii) *Scheme A*. We exclude black hole mass, while we apply the matching criteria on redshift, stellar mass, and environment.
- (iii) *Scheme B*. We exclude black hole mass, and environment, while we keep the criteria on redshift and stellar mass. Scheme B offers the closest matching criteria to those in Ellison et al. (2022),

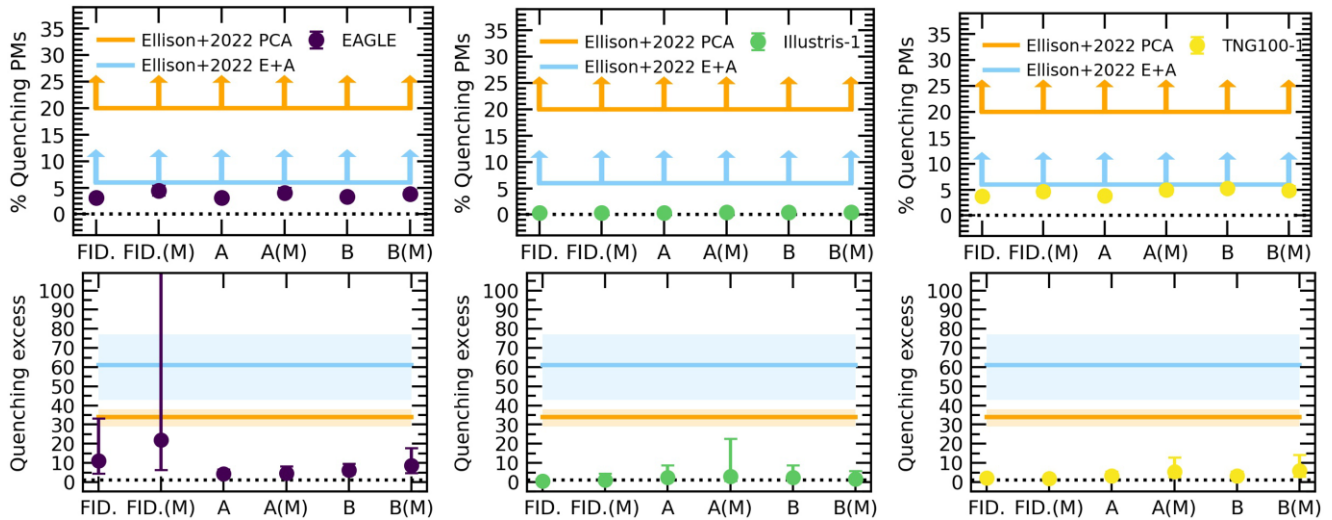


Figure 8. Top: comparison of the global quenched fraction in simulated post-mergers with the post-starburst fraction in mergers from observations in Ellison et al. (2022) (the arrows indicate that values are lower limits, the light blue line represents observed post-starbursts in mergers selected using a classical E+A method, whereas the orange line is for post-starbursts in mergers selected applying a PCA approach). Each panel is assigned to one of the three simulations, from left to right, EAGLE in purple, Illustris-1 in green, and TNG100-1 in yellow. Moreover, for each simulation, the comparison with observations is done using the outcome of six different matching schemes (see their definition in the text in Section 3.3). Bottom: comparison of the quenching excess in simulations with observations. The layout is the same as in the top panels. The figure depicts how the analysed cosmological simulations cannot quantitatively reproduce observational constraints of the impact of mergers on quenching star formation.

where each post-merger is matched to non-interacting galaxies in redshift and stellar mass.

Additionally, Ellison et al. (2022) found that post-mergers showing the most disturbed morphologies exhibit a higher post-starburst fraction. Because of the aforementioned reasons, it is likely that most observational post-starburst post-mergers might be remnants of major mergers. Therefore, for each of the three matching variations, we also perform an additional experiment with a focus only on major mergers (i.e. mass ratio $> 1:4$).

The result of the experiment is presented in the top panels of Fig. 8. The three top panels show, from left to right, the merger quenched fractions measured in the various matching scheme variations for EAGLE, Illustris-1, TNG100-1, respectively. In each panel, the merger quenched fractions from Ellison et al. (2022) are reported in orange and light blue, for the PCA and E+A selections, respectively. We also drew arrows to indicate that Ellison et al. (2022) values are lower limits for the reasons described earlier in this section.

3.3.1 Global quenched fraction

The top panels of Fig. 8 present the global quenched fractions of the three simulations. Symbols show the quenched fractions for the various matching schemes. Inspection of Fig. 8 reveals that EAGLE post-mergers (top left-hand panel) show quenched fractions between $3.1_{-0.4}^{+0.5}$ and $4.4_{-0.9}^{+1.1}$ per cent, with the larger values found in the variation scheme tests that are focused on major mergers. Illustris-1 shows, instead, quenched fractions between $0.3_{-0.2}^{+0.4}$ and $0.5_{-0.2}^{+0.3}$ per cent, values substantially smaller than observations in all the variation tests. Similarly to EAGLE, the quenched fraction in TNG100-1 post-mergers (top right-hand panel) are between $3.7_{-0.5}^{+0.6}$ and $5.3_{-0.7}^{+0.8}$ per cent. We note that TNG100-1 quenched fraction changed significantly from that in Fig. 5. Here, the TNG100-1 fraction goes down because of all the non-star-forming post-mergers introduced in the denominator.

The mild discrepancy between EAGLE, TNG100-1, and the E+A observational post-starburst fraction could be explained by a difference in quenching efficiency between simulations and observations. Previous works comparing simulations with observations show that the galaxy passive fraction is about 15 per cent too low in EAGLE (Furlong et al. 2015; Trayford et al. 2017). Also in Illustris-1 quenching is not efficient enough compared to observations (e.g. Sparre et al. 2015; Bluck et al. 2016; Terrazas et al. 2017), while the quenching mechanism is more efficient in TNG100-1 than previous simulations, hence showing a better agreement with observations (e.g. Donnari et al. 2019). The EAGLE and TNG100-1 quenched fractions seem to be quantitatively almost compatible with the lower limit of E+A selection (i.e. ~ 6 per cent), with TNG100-1 showing a slightly better agreement than EAGLE. However, they are both substantially smaller than the observational PCA post-starburst fraction (i.e. ~ 20 per cent), with a level of incompatibility that is arguably challenging to be explained by the different experimental set up.

We finally note that the quenched fractions in the three analysed matching schemes (i.e. fiducial, A, and B) do not substantially differ from each other because the adopted criteria do not compromise the completeness of the post-merger sample, that is stably above 90 per cent in all the three simulations regardless of the matching approach. Finally, it is interesting to note that the variation tests focused on the major merger subsamples show slightly larger quenched fractions than the corresponding tests on the whole merger sample, thus indicating that major mergers are more conducive to star formation quenching (see also Section 4.1).

3.3.2 Quenching excess

The second part of our comparison with observations regards the comparison of the quenching excess (i.e. the ratio between the number of quenched post-mergers over the number of quenched control galaxies) between simulated and observed mergers. Ellison

et al. (2022) found a strong statistical excess of post-starbursts in post-merger galaxies, with quenching being 34 to ~ 60 times (PCA and E+A selection, respectively) more common in post-mergers than in the control sample. The bottom panels of Fig. 8 show the quenching excess from our various matching scheme variations. The three panels refer, from left to right, to EAGLE, Illustris-1, and TNG100-1, respectively. In all the panels, we also report the observational excess of the PCA (in orange, with an excess of $\sim 34_{-5}^{+4}$) and E+A (in light blue, with an excess of $\sim 60_{-18}^{+16}$) selections from Ellison et al. (2022). None of the simulations has a quenching excess high enough to be comparable with the observations. EAGLE shows excess between $4.2_{-1.5}^{+2.4}$ and $22_{-15.9}^{+10.6}$ (in the scheme A and the fiducial scheme focused on major mergers, respectively). The latter, though compatible with observations within errors, have a very large uncertainty due to the paucity of quenched controls, i.e. only one quenched control galaxy versus 22 quenched post-mergers in the same period of time. Illustris-1 shows a post-merger quenching excess between $0.6_{-0.3}^{+0.7}$ and $3.0_{-2.4}^{+19.7}$, with values, on average, compatible with a deficit of quenching (i.e. quenching excess < 1), which means quenching in Illustris-1 post-mergers is less common than expected in a control sample, thus consistent with what we already found in Section 3.2. Finally, TNG100-1 shows a post-merger quenching excess between $2.0_{-0.6}^{+0.9}$ and $5.3_{2.9}^{+7.4}$ (in the fiducial matching scheme focused on major mergers and in the scheme A focused on major mergers), with a slightly worse agreement with observations than EAGLE. Earlier in this section, we demonstrated that the quenched fractions in EAGLE and TNG100-1 post-mergers are quantitatively almost compatible with the E+A selection, hence, the incommensurable difference in the quenching excess is driven by a larger number of control galaxies that quench in the simulations than in the observations. The difference in the simulated and observational controls could be explained if most of the simulated controls quench because of secular reasons and only a few pass through a post-starburst phase. However, we cannot test this speculative scenario because it would be challenging to isolate post-starburst galaxies in our global sample of mergers. Selecting a simulated sample of bona fide post-starbursts would require a different experimental approach and some fine-tuning to translate accurately the spectral post-starburst features into the star formation histories of the simulated galaxies (e.g. what should be the minimum strength of a burst to lead a galaxy through a post-starburst phase?).

To summarize, in this section, we attempt to compare the frequency of quenching in simulated and observed post-mergers. All of the three simulations, with the exception of a non-statistically robust EAGLE case, produce a much lower excess of rapidly quenching post-mergers compared with observations with a caveat that a robust comparison would need to consider the details of post-starburst galaxy selection versus just rapid quenching. The incompatibility between observations and simulations may indicate either missing physical ingredients in the simulations, or insufficient resolution to capture the merger-induced effects.

4 DISCUSSION

4.1 Lack of quenching in simulated post-mergers

So far, we have demonstrated that quenching of post-mergers in cosmological simulations occurs rarely and less frequently than in observations. However, we additionally demonstrate that the majority of star forming post-mergers have higher SMBH accretion rates compared with their controls and more frequently host highly accreting SMBHs, which suggests an excess of AGN feedback

activity. Here, we investigate pivotal parameters (i.e. M_{BH} , M_{halo} , mass ratio μ , and gas fraction f_{gas}) to get insights into the scarcity of quenching in simulated post-mergers. Before diving into the analysis, we present a brief overview of the importance of the aforementioned parameters on the interconnection between mergers and quenching.

Many studies indicate that black hole mass is the best physical proxy for determining the quenching status of massive galaxies, both in simulations (e.g. Bluck et al. 2016; Davies et al. 2019; Terrazas et al. 2020; Piotrowska et al. 2022), and observations (e.g. Bluck et al. 2016; Terrazas et al. 2016, 2017). In other words, black hole mass directly traces the integrated history of AGN feedback, hence, the cumulative energy released and coupled with the ISM and/or CGM. Quenched galaxies typically reside in massive haloes (e.g. Davies et al. 2019; Cui et al. 2021), harbour overmassive (i.e. massive for their halo mass) black holes and have a low gas fraction, with quenching starting when the total amount of energy from efficient AGN feedback overcomes the gravitational binding energy of the gas (e.g. Terrazas et al. 2020), and prevents the CGM from cooling and replenishing the gas reservoir that sustains star formation (e.g. Davies et al. 2020; Zinger et al. 2020).

Quai et al. (2021) empirically found that gas fraction (i.e. the fraction of the total gas over the sum of stellar and gas mass within an aperture of two effective radii) is the best indicator for quenching in TNG300-1's galaxies, with star formation halting sharply as soon as gas fraction falls below 0.1 due to the ejective effect of the TNG kinetic mode feedback. In this work, we generalize Quai et al. (2021)'s findings to the EAGLE, Illustris-1, and TNG100-1 simulations.

It is well established that mass ratio plays an important role in the impact of mergers on star formation (e.g. Cox et al. 2008; Moreno et al. 2015; Zheng et al. 2020). About 50 per cent of our post-mergers in the three simulations consist of minor mergers (i.e. $\mu < 0.25$, see the bottom left-hand panel in Fig. 1), hence, it is necessary to tackle whether and how much our results are influenced by mass ratio. Altogether, the aforementioned parameters allow us to better understand the interplay between mergers, black holes, and star formation.

The result of the analysis is shown in Fig. 9 for EAGLE, in Fig. 10 for Illustris-1, and in Fig. 11 for TNG100-1. The figures show the distribution (from top to bottom) of M_{halo} , gas fraction f_{gas} , and mass ratio μ as a function of black hole mass of star-forming (blue points), green valley (green points), and quenching (red points) post-mergers at 500 Myr after coalescence. Moreover, the histogram in the top panel of each figure shows the percentage distribution of post-mergers in bins of black hole mass, whilst the three panels on the right show the histograms of the percentage distribution of post-mergers in bins of (from top to bottom) M_{halo} , f_{gas} , and μ . We discuss the results for each simulation in turn.

4.1.1 EAGLE

We discuss the results starting from the analysis of EAGLE in Fig. 9. The histogram in the top panel demonstrates that quenching in EAGLE post-mergers is rare in any black hole mass regime. Almost all quenched post-mergers have black hole masses between $10^{7.1}$ and $10^{8.25} M_{\odot}$, although, this mass regime is dominated by star-forming post-mergers, representing 60–80 per cent of the population. At lower black hole mass, we find a long tail of 740 (i.e. the 55 per cent of EAGLE post-mergers) galaxies, out of which only 3 and 18 are quenched and green valley post-mergers, respectively. However, at

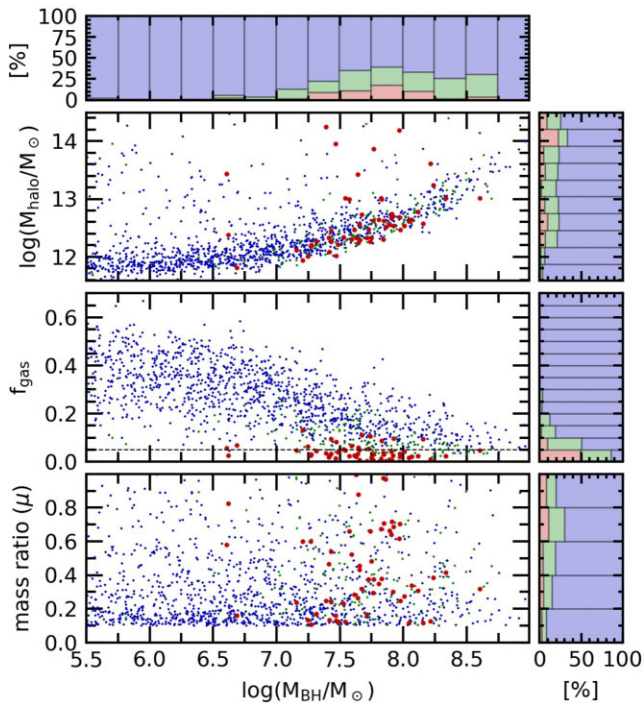


Figure 9. The three main panels show, from top to bottom, the halo mass ($\log(M_{\text{halo}}/M_{\odot})$), the gas fraction (f_{gas}), and the mass ratio (μ) as a function of the black hole mass ($\log(M_{\text{BH}}/M_{\odot})$) for EAGLE post-mergers at 500 Myr after the merger. Star-forming post-mergers are represented in blue, green valley post-mergers are represented in green, and quenched post-mergers in red. The histogram above the top panel shows the percentage distribution of star-forming, green valley, and quenched post-mergers in bins of black hole mass. The histograms at the right-hand side of the main panels represent the percentage distributions of post-mergers in bins of, from top to bottom, halo mass, gas fraction, and mass ratio. The figure shows that the vast majority of EAGLE post-mergers do not quench, mostly because they have small black holes, but also because some of them reside in massive haloes in which the AGN feedback is not able to interrupt the cooling of dense gas in the centre of their circumgalactic medium (read Appendix A in Davies et al. 2019).

black hole masses larger than $10^{8.25} M_{\odot}$, where we would expect the quenched population to prevail, we find that 73 per cent of post-mergers are star-forming, and only 2 out of 94 are quenched.

To better understand why EAGLE post-mergers do not quench promptly, we investigate the $M_{\text{halo}}-M_{\text{BH}}$ and $f_{\text{gas}}-M_{\text{BH}}$ relationships (top and central distributions, respectively, in Fig. 9). All post-mergers with less massive black holes reside in small haloes and have gas fractions large enough to keep sustaining new episodes of star formation. In this black hole mass regime, it is clear that AGN feedback is not effective² in removing gas from the ISM, and the low virial temperature and high CGM mass fraction (and hence characteristic density of the CGM) of the haloes grants short cooling time, thus providing fuel for star formation. It is less straightforward to interpret the dearth of quenching in post-mergers with black holes more massive than $10^{8.25} M_{\odot}$. The extra complication arises because EAGLE’s AGN feedback is not efficient enough at ejecting baryons and preventing cooling in group and cluster haloes. This is the reason why the EAGLE model produces groups and clusters that are too

²The modified Bondi–Hoyle accretion implemented in EAGLE is proportional to M_{BH} (Rosas-Guevara et al. 2015, 2016).

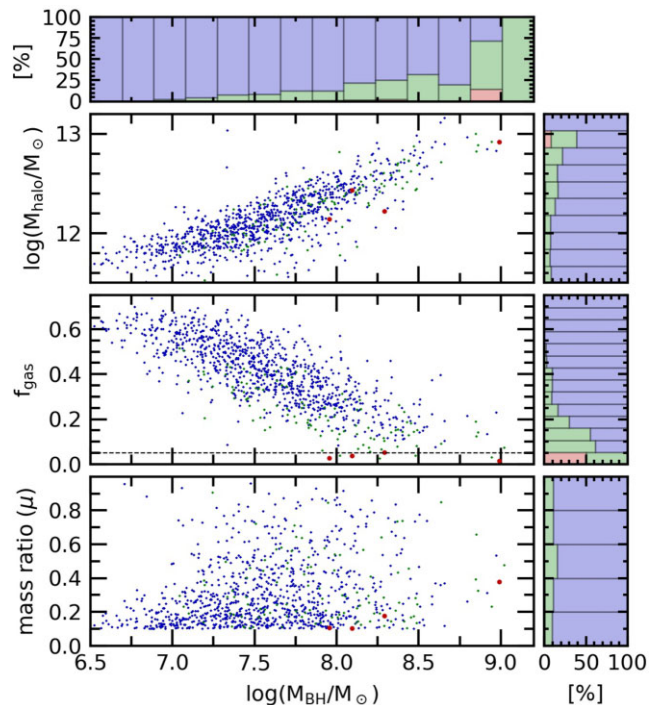


Figure 10. Same as in Fig. 9, but for Illustris-1. Note that the range in black hole masses differs from that in Fig. 9, due to the difference in black hole mass distribution between EAGLE and Illustris-1 post-mergers (see Fig. 1). The figure shows that only four Illustris-1 post-mergers quench star formation within 500 Myr after coalescence. The fraction of green valley post-mergers increases with increasing halo and black hole mass. However, quenching happens only in the few galaxies showing a gas fraction as low as 0.05 or less. The mass ratio does not affect the quenching fraction. Indeed, the fraction of green valley galaxies does not increase with the increasing mass ratio.

bright in X-ray (see Appendix A in Schaye et al. 2015; Davies et al. 2019). The CGM mass fraction is high in these haloes, hence, their inner regions can become quite dense, giving a short cooling time (see Davies et al. 2019; Oppenheimer et al. 2020). It is then very difficult for the AGN to remove gas from the CGM, which can therefore replenish the galaxy supply for new star formation.

We can observe the effect of change in AGN ‘effectiveness’ by looking at the $f_{\text{gas}}-M_{\text{BH}}$ distribution, and at the histogram of the percentage distribution of post-mergers in bins of f_{gas} in the central panels of Fig. 9. The panels show a trend with f_{gas} reducing with increasing M_{BH} (and increasing M_{halo}). However, the vast majority of post-mergers maintain $f_{\text{gas}} > 0.05$, thus being able to form stars and stay in the star-forming main sequence. The few post-mergers that quench within 500 Myr after coalescence have gas fraction around or below 0.05.

In the bottom panel of Fig. 9, we investigate how the merger mass ratio influences the quenched fraction in EAGLE post-mergers. We find that major mergers show a slightly larger chance to be quenched, but even at mass ratios $\mu > 0.7$, only a small fraction of 7.3 per cent post-mergers are quenched, to which can be added 15.3 per cent of post-mergers in the green valley.

The weak dependence of quenched fraction on merger mass ratio is in contrast with some other results in the literature. For instance, Davies et al. (2022) found that increasing mass ratio in a EAGLE Milky Way-like merger galaxy causes more violent and preferentially head-on collisions, maximizing the probability of quenching star

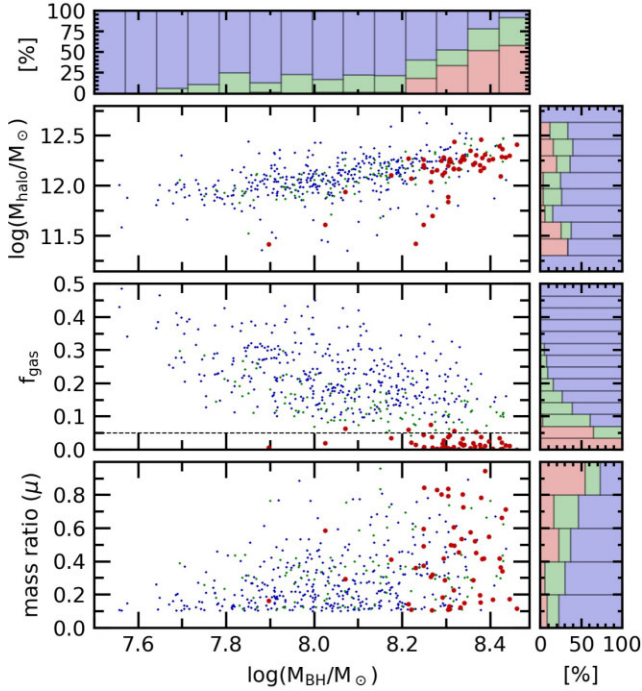


Figure 11. Same as in Fig. 9, but for TNG100-1. Note that the range in black hole masses differs from that in Fig. 9, due to the difference in black hole mass distribution between EAGLE and TNG100-1 post-mergers (see Fig. 1). The figure shows that the importance of quenching in TNG100-1 post-mergers starts arising at black hole masses above $10^{8.2} M_{\odot}$, the black hole mass threshold above which more than 90 per cent of the TNG galaxies are quenched (e.g. Terrazas et al. 2020; Zinger et al. 2020). However, quenching occurs only in those post-mergers with massive black holes that have also a very low gas fraction, $f_{\text{gas}} \leq 0.05$ (see also Quai et al. 2021). The figure shows also that major mergers have a larger chance to quench star formation.

formation. If we limit the analysis to Milky Way-like post-mergers with $12.5 \leq \log(M_{\text{halo}}/M_{\odot}) \leq 12.7$, we find that major mergers ($\mu > 0.5$) have around 20 per cent higher chance to quench (or to reside in the green valley) shortly after coalescence than in minor mergers. Although, we also find that as much as 63 per cent of galaxies in this regime (i.e. major mergers in Milky Way-like galaxies) keep to stay star-forming.

To summarize, in EAGLE we find that as halo mass increases, the chances of a galaxy to be quenched by AGN feedback increases up to $M_{\text{BH}} \sim 10^{8.2} M_{\odot}$, and then decreases as the AGN stop being effective in massive haloes. Moreover, we do not find a significant impact of the merger mass ratio on the quenched fraction of EAGLE post-merger galaxies. Ultimately, we find that the gas fraction is the key ingredient to clearly disentangle star-forming and quenched post-mergers.

4.1.2 Illustris-1

Fig. 10 shows the results regarding Illustris-1. The figure demonstrates that only four Illustris-1 post-mergers quench within 500 Myr after the merger. Despite the fact that the gas fraction decreases steadily with increasing black hole mass (and increasing halo mass), the star formation is affected (there is an increasing number of green valley galaxies), though not completely halted. The implementation of the Illustris-1 AGN feedback is the reason for such complete lack of quenching in post-mergers. Indeed, Illustris-1 post-mergers

show a strong black hole accretion enhancement (see Section 3.1), thus activating the high accretion mode of the AGN feedback, which deposits thermal energy with a low coupling efficiency (e.g. Sparre et al. 2015; Bluck et al. 2016; Terrazas et al. 2017; Donnari et al. 2019), leaving the surrounding ISM almost unaffected.

4.1.3 TNG100-1

We focus now on the analysis of the lack of quenching in TNG100-1's post-mergers. The results are shown in Fig. 11, with an identical layout as that in Fig. 9 for EAGLE. Studies of quenching in TNG (Nelson et al. 2017; Weinberger et al. 2017; Terrazas et al. 2020) demonstrated that only the kinetic mode of AGN feedback is capable of causing star formation suppression. Terrazas et al. (2020) showed that the ejective feedback in TNG becomes effective at quenching star formation once the cumulative kinetic energy overcomes the total gravitational binding energy of the gas in a galaxy. They also demonstrated that the kinetic feedback process dominates in galaxies whose M_{BH} exceeds $10^{8.2} M_{\odot}$, that is the black hole mass threshold above which more than 90 per cent of the TNG galaxies are quenched (see also Zinger et al. 2020). Such a M_{BH} threshold for quiescence arises from the TNG model parameters chosen to reproduce observational properties of the galaxy population at present (Pillepich et al. 2017a). Our results concerning the quenching deficiency in the TNG100-1 post-merger population reflect the general quenching process of galaxies in the simulation. In detail, the histogram in the top panel of Fig. 11 shows that almost none of the post-mergers with $M_{\text{BH}} < 10^{8.2} M_{\odot}$ are quenching, whilst the percentage of quenched post-mergers increases steadily at larger black hole mass, passing from 18 per cent at $M_{\text{BH}} \sim 10^{8.3} M_{\odot}$, to 58 per cent at $M_{\text{BH}} \sim 10^{8.4} M_{\odot}$, to which we can add, respectively, 22 per cent and 33 per cent of post-mergers in the green valley. All TNG quenched post-mergers have gas fraction $f_{\text{gas}} \leq 0.05$ (see the central panels in Fig. 11), confirming that these galaxies ran out of fuel for star formation. Differently from EAGLE though, we do not find trends with M_{halo} (see the top panels in Fig. 11). However, our TNG100-1 post-merger population has a smaller mass dynamical range, with most of the massive galaxies residing in haloes of around $10^{12.5} M_{\odot}$, hence, we cannot probe the quenching efficiency of TNG AGN feedback in post-mergers located in groups and clusters, as we can do for the EAGLE sample.

In the bottom panels of Fig. 11, we investigate whether merger mass ratio influences the quenched fraction in TNG100-1 post-mergers. The histogram in the bottom right-hand corner shows that the percentage of quenched post-mergers strongly increases with increasing mass ratio, with a peak of 55 per cent quenched post-mergers in the bin of mass ratio above 0.8. However, the distribution of mass ratio as a function of black hole mass (bottom left-hand panel of Fig. 11) shows a trend where higher mass ratio mergers have larger black hole mass, thus with a higher AGN feedback efficiency. To test whether the increment of the quenched fraction with the mass ratio is attributable to a larger black hole population, we calculate the fraction of quenched galaxies in two bins of mass ratio (i.e. $\mu \leq 0.5$, and $\mu > 0.5$) for a subsample of TNG100-1 post-mergers that have black holes more massive than $10^{8.2} M_{\odot}$. In this subsample, we find 28.4 per cent and 41.9 per cent of quenched post-mergers in the minor and major merger bins, respectively, thus suggesting that TNG100-1 major mergers increase the chance of quenching shortly after coalescence. However, we find that as much as 39.5 per cent of major mergers that exhibit a massive black hole continue to reside in the star-forming main sequence. Such lack of quenching in major mergers could be due to other parameters

governing the evolution in post-merger phases. For instance, Zeng, Wang & Gao (2021) showed that progenitor orbits have an important effect on the remnant of TNG100-1 post-mergers, with prograde orbits resulting in post-mergers with a high chance to preserve the original disc and a star-forming configuration even in major merger events.

To summarize, we find that quenching in a TNG100-1 post-merger occurs promptly after coalescence only if its black hole mass is larger than $\sim 10^{8.2} M_{\odot}$ (i.e. the mass above which the TNG100-1’s AGN feedback switches to the effective kinetic mode; Weinberger et al. 2018; Terrazas et al. 2020), and at the same time, its gas fraction is below 0.05. We also find that the TNG100-1 quenching fraction increases with increasing mass ratio, even though around 40 per cent of major mergers harbouring massive black holes continue to be star-forming long after coalescence.

4.2 Gas loss

In the previous sections, we showed that most simulated post-mergers keep forming stars. However, even if quenching is less frequent than in observations, we find that post-mergers quench at circa twice and at around ten times the rate of non-interacting control galaxies, in TNG100-1 and EAGLE, respectively (see Fig. 6).

In the previous section the role of effective AGN feedback in quenched EAGLE and TNG100-1 post-mergers was investigated, a process which is in common with non-interacting galaxies. However, since we matched the two populations (and kept the match over the entire simulation life) in black hole mass (see Section 2.4), the quenching excess cannot be completely attributable to a mere difference in the black hole population, hence, it could be related to the merger process itself. In this section, we aim to tackle the origin of the extra quenching in EAGLE and TNG100-1 post-mergers. Note that we do not further analyse Illustris-1’s post-mergers because in Section 3.2 we demonstrated that quenched post-mergers in Illustris-1 are rarer than what expected from control non-interacting galaxies.

In Figs 9, 10, 11, it emerged that gas fraction is an excellent discriminator for the star-formation status of a population. Particularly, we found that a low level of gas fraction (i.e. $f_{\text{gas}} \leq 0.05$) strongly correlates with quenching. To shed light on the surplus of quenching in post-mergers compared to their direct control galaxies, it is, therefore, worth investigating how gas fraction evolves from coalescence in the post-merger population. We present the results in Fig. 12. The two panels show the gas fraction at 500 Myr after the merger versus the gas fraction at coalescence for (from top to bottom) EAGLE and TNG100-1. Star-forming post-mergers are represented in blue, green valley post-mergers in green and quenched post-mergers in red. The inset in each panel shows the distributions of gas loss, Δf_{gas} (i.e. $f_{\text{gas}} [t_{\text{pm}} = 0.5 \text{ Gyr}] - f_{\text{gas}} [t_{\text{pm}} = 0]$), of the three star formation categories (i.e. star-forming, green valley, and quenched). We find two key results from the analysis of Fig. 12. First of all, the plot shows that 82.5 per cent and 91 per cent (in EAGLE and TNG100-1, respectively) of quenched post-mergers had low gas fractions at coalescence,³ with values $f_{\text{gas}} \leq 0.2$. Such low gas fraction values at the time of the merger suggest that there is a pre-disposition towards quenching when the gas fraction is low to start with (see also Quai et al. 2021). What is also interesting is that the distributions of Δf_{gas} shown in the insets of Fig. 12 demonstrate that quenched post-mergers in both simulations are also experiencing ‘preferentially’

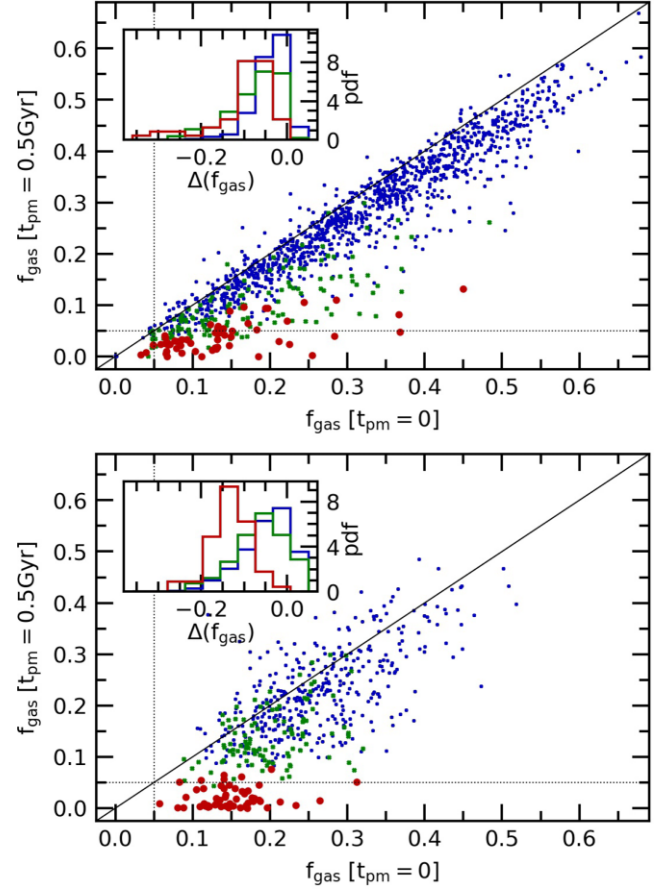


Figure 12. Distribution of gas fraction at 500 Myr after the merger versus the gas fraction at coalescence. The top panel shows the result for the EAGLE simulation, whilst the bottom panel is for the TNG100-1 simulation. Star-forming post-mergers are represented in blue, green valley post-mergers in green, whilst quenched post-mergers in red. The insets in both panels represent the distribution of Δf_{gas} (i.e. $f_{\text{gas}} [t_{\text{pm}} = 0.5 \text{ Gyr}] - f_{\text{gas}} [t_{\text{pm}} = 0]$). The panels show that two things are necessary to quench post-merger galaxies in both simulations: (1) a predisposition towards quenching (i.e. most of the quenched post-mergers have small gas fraction to start with), and (2) experience a large amount of gas loss shortly after the merger.

larger gas loss compared to those that stay star-forming and in the green valley. In numbers, we find mean values of $\Delta f_{\text{gas}} = -0.1$ and $= -0.13$ for EAGLE and TNG100-1 quenched post-mergers, respectively. Conversely, we find mean values of $\Delta f_{\text{gas}} = -0.03$ for both EAGLE and TNG100-1 star-forming, and $\Delta f_{\text{gas}} = -0.07$ and $= -0.06$ for EAGLE and TNG100-1 green valley post-mergers. Therefore, on the one hand, there is a ‘pre-disposition’ to quench. However, on the other hand, the quenched post-mergers tend to lose relatively more gas shortly after coalescence.

We investigate further the latter hypothesis in Fig. 13, as well as attempting to quantify the mechanism responsible for the gas depletion that leads to quenching. Each vertical bar represents a single post-merger that quenches within 500 Myr after the merger. In the top panel we focus on EAGLE, while quenched post-mergers in TNG100-1 are presented in the bottom panel. Galaxies are sorted from right to left from lowest to highest $-\Delta f_{\text{gas}}$ values (dark red histogram-like distribution), or in other words, according to increasing amount of gas missing with respect to coalescence. For each galaxy, we then show the percentage of such gas that has been

³We stress that at coalescence all the galaxies in our samples have to be star forming by construction, see Section 2.

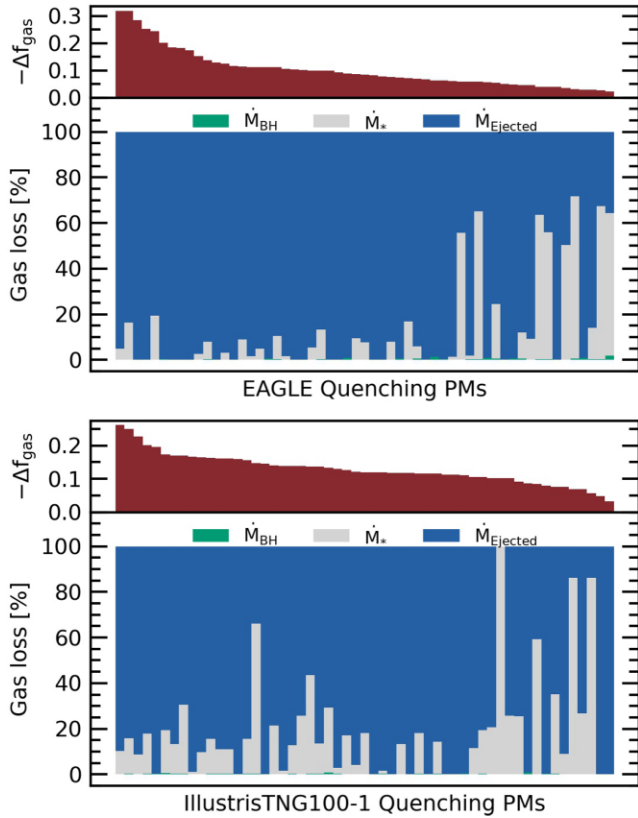


Figure 13. In the top panel, each vertical line represents a single EAGLE quenched post-merger, whilst in the bottom panel, each vertical line represents a single TNG100-1 quenched post-merger. Galaxies are sorted from right to left from lowest to highest $-\Delta f_{\text{gas}}$ values (dark red distribution in the top of both panels), which means according to the increasing amount of gas missing. Then, for each galaxy we split the percentage of gas loss into three groups: (1) gas that has been accreted onto the central black hole (green bar), (2) gas that has been converted into new stars (grey bar), and (3) gas that has been pushed out of the galaxy (blue bar).

accreted onto the central black hole (green bar; almost invisible for most galaxies), that has been converted into new stars (grey bar), and the percentage of gas that has been ejected outside the galaxy (blue bar). Fig. 13 shows that in both simulations there is a large predominance of post-mergers which have $> 80 - 100$ per cent of their missing gas completely ejected out of the galaxy, especially at higher $-\Delta f_{\text{gas}}$ values.

In summary, in this section we uncovered the two most common scenarios through which post-mergers quench following a merger event: galaxies which are predisposed to quench due to low gas fractions and those that quench after a period of significant gas evacuation.

4.3 Rapid versus long-term quenching

In this work we probed a merger-driven quenching scenario within state-of-the-art hydrodynamical cosmological simulations that encompass complete and robust samples of mergers covering a wide range of halo mass, mass ratio, orbital parameters, physical properties, and environment. We found that a prompt quenching following a merger event is much less frequent than that expected from observational results and previous generations of simulations (see also

Weinberger et al. 2018; Rodríguez Montero et al. 2019; Pathak et al. 2021, for similar results). We limited our analysis to the early stages of the post-merger evolution (i.e. probing the causal connection between mergers and rapid quenching) for two reasons: (1) the quenched fraction in post-mergers tends to gradually level off and finally even out with the quenched fraction of the control population (i.e. post-merger evolution becomes statistically indistinguishable from the secular evolution of non-interacting galaxies, see Figs 5 and 6); and (2) observations of quenched post-mergers are confined within a few hundred Myr after the coalescence phase. However, we cannot exclude the possibility of a long-term quenching that might be causally connected to galaxy–galaxy interactions. For instance, Davies et al. (2022) showed that in a series of genetically modified mergers of Milky Way-like galaxies from the EAGLE simulation, the intense AGN feedback triggered by major mergers can modify the evolution of the galaxy–CGM ecosystem. In such controlled post-mergers, the AGN feedback can eject enough gas to promptly push the galaxy out of the main sequence but not to fully quench its star formation. Quenching arises typically only around 3 Gyr after the merger, due to the prolonged CGM cooling time that prevents further inflow of new gas. Testing longer term quenching observationally is much more of a challenge as it requires being able to time the quenching episode as well as timing merger features (to prove a causal connection between them). Whilst star formation histories might be able to give fairly reliable quenching times in the last few Gyr, timing mergers is harder, although some machine learning applications are now attempting to do this (e.g. Bottrell et al. 2022; Bottrell et al., in preparation).

5 SUMMARY AND CONCLUSIONS

We have used three different cosmological simulations to analyse a complete sample of post-merger galaxies in a fully cosmological environment spanning a diverse range of merger histories and physical properties. Each simulation implements accretion onto the central supermassive black hole and AGN feedback models that are distinct (see, for instance, Section 2).

Although galaxy–galaxy mergers are rare events in the history of a galaxy, there is a general consensus that mergers have a tremendous impact on the evolution of the merger remnants, with repercussions on shaping the global properties of galaxies (e.g. dark and stellar mass increment, metallicity evolution, mass function evolution, etc.). Such relative importance of mergers in the bigger picture of galaxy evolution should naturally arise as predictions of the models implemented in simulations. In this paper, we quantify the effect of galaxy–galaxy mergers on the black hole accretion, AGN feedback, and rapid star formation quenching in three state-of-the-art cosmological simulations: EAGLE, Illustris-1, and TNG100-1. Moreover, for the first time we can compare the incidence of quenching in simulations with that of a large and pure sample of observed post-merger galaxies analysed in Ellison et al. (2022). Our findings can be summarized as follows:

(i) The majority of star forming post-mergers exhibit higher SMBH accretion rates when compared with matched controls. On average, the post-merger population exhibits SMBH accretion rates 2.5 (EAGLE), 4.5 (Illustris-1), and 2.1 (TNG100-1) times higher than matched controls (see Section 3.1, and Figs 2 and 3).

(ii) Highly accreting SMBHs occur more frequently in the post-merger sample compared to the control sample, where post-mergers host the highest SMBH accretion rates up to four times more often (see Fig. 4).

(iii) Rapid quenching is rare in the post-merger population in all three cosmological simulations. Only 4.5 per cent (EAGLE), 0.4 per cent (Illustris-1), and 10 per cent (TNG100-1) of post-mergers quench within 500 Myr of coalescence (see Section 3.2 and Fig. 5). Despite the rarity of quenched post-mergers, quenching occurs more frequently than in the control population in the EAGLE and TNG100-1 simulations, with maximum quenching excesses factor (for the fiducial matching scheme) of 11 and 2, respectively. In contrast, Illustris-1 demonstrates a quenching deficit, such that more control galaxies quench compared with the post-merger population (see Fig. 6).

(iv) We proved the lack of a rapid merging-driven quenching scenario. However, we cannot statistically rule out a possible long-term quenching (over a few Gyr after coalescence) due, for instance, to a prolonged cooling time of the circumgalactic medium. For such long time-scales we find that in all three simulations quenching in the post-merger population is statistically indistinguishable from the control sample of non-interacting galaxies, thus preventing any attempt to causally connect long quenching to merger itself (see Figs 5 and 6, and comments in Section 4.3).

(v) We compare our results with the observational results of Ellison et al. (2022), looking at the quenched fraction and quenching excess in post-starburst galaxies. We find the quenched fractions of EAGLE and Illustris-1 to be almost comparable to the lower limit estimated from E+A post-starburst selection, but incompatible with the lower limit estimated from PCA post-starburst selection. We further find that the simulations generally fail to reproduce the quenching excess of Ellison et al. (2022), with a note that EAGLE is able to produce an excess in agreement with Ellison et al. (2022) but with poor statistical significance (see Section 3.3, and Fig. 8).

(vi) We investigate the rarity of quenching in the post-merger population and find that the majority of post-mergers retain a significant amount of gas in the 500 Myr following coalescence, providing sufficient fuel for sustaining star formation (see Section 4, and Figs 9, 10, and 11).

(vii) We further demonstrate that there are two mechanisms at play to quench post-mergers: (1) a predisposition for post-mergers to quench if they exhibit a low gas fractions at the time of coalescence, and (2) a large amount of gas ejected promptly within 500 Myr of coalescence (see Section 4.2, and Figs 12 and 13).

ACKNOWLEDGEMENTS

We thank the referee, Neven Caplar, for his useful comments. We would like to express our gratitude to Jonathan J. Davies for his constructive comments and suggestions that greatly contributed to this work and Stuart McAlpine for providing the private-available EAGLE snippets galaxy catalogue and insightful discussions. We are also grateful to Andrew Pontzen for his useful comments and suggestions. DRP and SLE gratefully acknowledge NSERC for Discovery Grants which helped to fund this research. This research was enabled, in part, by the computing resources provided by WestGrid and Compute Canada.

DATA AVAILABILITY

The data used in this work have been previously published. TNG100-1 and Illustris-1 data are publicly available at <https://www.tng-project.org>, and www.illustris-project.org/, respectively. EAGLE data, instead, can be accessed via <https://virgodb.dur.ac.uk>, however the snippets used in this paper are for internal use only.

REFERENCES

- Alonso M. S., Lambas D. G., Tissera P., Coldwell G., 2007, *MNRAS*, 375, 1017
- Barnes J. E., Hernquist L., 1996, *ApJ*, 471, 115
- Bekki K., Couch W. J., Shioya Y., Vazdekis A., 2005, *MNRAS*, 359, 949
- Bessiere P. S., Tadhunter C. N., Ramos Almeida C., Villar Martín M., 2012, *MNRAS*, 426, 276
- Bickley R. W., Ellison S. L., Patton D. R., Bottrell C., Gwyn S., Hudson M. J., 2022, *MNRAS*, 514, 3294
- Blake C. et al., 2004, *MNRAS*, 355, 713
- Bluck A. F. L. et al., 2016, *MNRAS*, 462, 2559
- Blumenthal K. A., Barnes J. E., 2018, *MNRAS*, 479, 3952
- Bondi H., 1952, *MNRAS*, 112, 195
- Bondi H., Hoyle F., 1944, *MNRAS*, 104, 273
- Booth C. M., Schaye J., 2009, *MNRAS*, 398, 53
- Bottrell C., Hani M. H., Teimoorinia H., Patton D. R., Ellison S. L., 2022, *MNRAS*, 511, 100
- Bower R. G., Benson A. J., Malbon R., Helly J. C., Frenk C. S., Baugh C. M., Cole S., Lacey C. G., 2006, *MNRAS*, 370, 645
- Bustamante S., Sparre M., Springel V., Grand R. J. J., 2018, *MNRAS*, 479, 3381
- Bustamante S., Ellison S. L., Patton D. R., Sparre M., 2020, *MNRAS*, 494, 3469
- Byrne-Mamahit S., Hani M. H., Ellison S. L., Quai S., Patton D. R., 2022, *MNRAS*, available at: <https://doi.org/10.1093/mnras/stac3674>
- Cao C. et al., 2016, *ApJS*, 222, 16
- Capelo P. R., Volonteri M., Dotti M., Bellovary J. M., Mayer L., Governato F., 2015, *MNRAS*, 447, 2123
- Casteels K. R. V. et al., 2014, *MNRAS*, 445, 1157
- Cattaneo A. et al., 2009, *Nature*, 460, 213
- Chabrier G., 2003, *PASP*, 115, 763
- Cisternas M. et al., 2011, *ApJ*, 741, L11
- Citro A., Pozzetti L., Quai S., Moresco M., Vallini L., Cimatti A., 2017, *MNRAS*, 469, 3108
- Correa C. A., Schaye J., Trayford J. W., 2019, *MNRAS*, 484, 4401
- Couch W. J., Sharples R. M., 1987, *MNRAS*, 229, 423
- Cox T. J., Jonsson P., Somerville R. S., Primack J. R., Dekel A., 2008, *MNRAS*, 384, 386
- Crain R. A. et al., 2015, *MNRAS*, 450, 1937
- Croton D. J. et al., 2006, *MNRAS*, 365, 11
- Cui W., Davé R., Peacock J. A., Anglés-Alcázar D., Yang X., 2021, *Nat. Astron.*, 5, 1069
- Davies J. J., Crain R. A., McCarthy I. G., Oppenheimer B. D., Schaye J., Schaller M., McAlpine S., 2019, *MNRAS*, 485, 3783
- Davies J. J., Crain R. A., Oppenheimer B. D., Schaye J., 2020, *MNRAS*, 491, 4462
- Davies J. J., Pontzen A., Crain R. A., 2022, *MNRAS*, 515, 1430
- De Propriis R., Conselice C. J., Liske J., Driver S. P., Patton D. R., Graham A. W., Allen P. D., 2007, *ApJ*, 666, 212
- Di Matteo T., Springel V., Hernquist L., 2005, *Nature*, 433, 604
- Di Matteo P., Combes F., Melchior A.-L., Semelin B., 2007, *A&A*, 468, 61
- Di Matteo T., Colberg J., Springel V., Hernquist L., Sijacki D., 2008, *ApJ*, 676, 33
- Donnari M. et al., 2019, *MNRAS*, 485, 4817
- Dressler A., Gunn J. E., 1983, *ApJ*, 270, 7
- Ellison S. L., Patton D. R., Simard L., McConnachie A. W., 2008, *AJ*, 135, 1877
- Ellison S. L., Patton D. R., Mendel J. T., Scudder J. M., 2011, *MNRAS*, 418, 2043
- Ellison S. L., Mendel J. T., Scudder J. M., Patton D. R., Palmer M. J. D., 2013a, *MNRAS*, 430, 3128
- Ellison S. L., Mendel J. T., Patton D. R., Scudder J. M., 2013b, *MNRAS*, 435, 3627
- Ellison S. L., Viswanathan A., Patton D. R., Bottrell C., McConnachie A. W., Gwyn S., Cuillandre J.-C., 2019, *MNRAS*, 487, 2491
- Ellison S. L. et al., *MNRAS*, 2022, 517, L92
- Fabian A. C., Celotti A., Erlund M. C., 2006, *MNRAS*, 373, L16

- Furlong M. et al., 2015, *MNRAS*, 450, 4486
 Gao F. et al., 2020, *A&A*, 637, A94
 Gehrels N., 1986, *ApJ*, 303, 336
 Goto T., 2005, *MNRAS*, 357, 937
 Goulding A. D. et al., 2018, *PASJ*, 70, S37
 Grønnow A. E., Finlator K., Christensen L., 2015, *MNRAS*, 451, 4005
 Habouzit M. et al., 2021, *MNRAS*, 503, 1940
 Habouzit M. et al., 2022, *MNRAS*, 509, 3015
 Hani M. H., Ellison S. L., Sparre M., Grand R. J. J., Pakmor R., Gomez F. A., Springel V., 2019, *MNRAS*, 488, 135
 Hani M. H., Gosain H., Ellison S. L., Patton D. R., Torrey P., 2020, *MNRAS*, 493, 3716
 Hernández-Toledo H. M., Avila-Reese V., Conselice C. J., Puerari I., 2005, *AJ*, 129, 682
 Hernquist L., 1989, *Nature*, 340, 687
 Hewlett T., Villforth C., Wild V., Mendez-Abreu J., Pawlik M., Rowlands K., 2017, *MNRAS*, 470, 755
 Hinshaw G. et al., 2013, *ApJS*, 208, 19
 Hopkins P. F., Hernquist L., Cox T. J., Kereš D., 2008, *ApJS*, 175, 356
 Hoyle F., Lyttleton R. A., 1940, *Proc. Camb. Phil. Soc.*, 36, 325
 Kennicutt Robert C. J., 1998, *ApJ*, 498, 541
 Khalatyan A., Cattaneo A., Schramm M., Gottlöber S., Steinmetz M., Wisotzki L., 2008, *MNRAS*, 387, 13
 Knapen J. H., Cisternas M., Querejeta M., 2015, *MNRAS*, 454, 1742
 Kocevski D. D. et al., 2012, *ApJ*, 744, 148
 Kocevski D. D. et al., 2015, *ApJ*, 814, 104
 Lambrides E. L. et al., 2021, *ApJ*, 919, 129
 Li C., Kauffmann G., Heckman T. M., Jing Y. P., White S. D. M., 2008, *MNRAS*, 385, 1903
 Lotz J. M., Jonsson P., Cox T. J., Primack J. R., 2008, *MNRAS*, 391, 1137
 Lynden-Bell D., 1969, *Nature*, 223, 690
 Marian V. et al., 2020, *ApJ*, 904, 79
 Marinacci F. et al., 2018, *MNRAS*, 480, 5113
 McAlpine S. et al., 2016, *Astron. Comput.*, 15, 72
 McAlpine S., Harrison C. M., Rosario D. J., Alexander D. M., Ellison S. L., Johansson P. H., Patton D. R., 2020, *MNRAS*, 494, 5713
 Mihos J. C., 1995, *ApJ*, 438, L75
 Mihos J. C., Hernquist L., 1996, *ApJ*, 464, 641
 Montuori M., Di Matteo P., Lehnert M. D., Combes F., Semelin B., 2010, *A&A*, 518, A56
 Moreno J., Torrey P., Ellison S. L., Patton D. R., Bluck A. F. L., Bansal G., Hernquist L., 2015, *MNRAS*, 448, 1107
 Murray N., Quataert E., Thompson T. A., 2005, *ApJ*, 618, 569
 Naiman J. P. et al., 2018, *MNRAS*, 477, 1206
 Nelson D. et al., 2015, *Astron. Comput.*, 13, 12
 Nelson D. et al., 2017, *MNRAS*, 475, 624
 Oegerle W. R., Hill J. M., Hoessel J. G., 1991, *ApJ*, 381, L9
 Oppenheimer B. D. et al., 2020, *ApJ*, 893, L24
 Pakmor R., Springel V., Bauer A., Mocz P., Munoz D. J., Ohlmann S. T., Schaal K., Zhu C., 2016, *MNRAS*, 455, 1134
 Pathak D., Belli S., Weinberger R., 2021, *ApJ*, 916, L23
 Patton D. R., Grant J. K., Simard L., Pritchett C. J., Carlberg R. G., Borne K. D., 2005, *AJ*, 130, 2043
 Patton D. R., Torrey P., Ellison S. L., Mendel J. T., Scudder J. M., 2013, *MNRAS*, 433, L59
 Patton D. R., Qamar F. D., Ellison S. L., Bluck A. F. L., Simard L., Mendel J. T., Moreno J., Torrey P., 2016, *MNRAS*, 461, 2589
 Patton D. R. et al., 2020, *MNRAS*, 494, 4969
 Pawlik M. M. et al., 2018, *MNRAS*, 477, 1708
 Pawlik M. M., McAlpine S., Trayford J. W., Wild V., Bower R., Crain R. A., Schaller M., Schaye J., 2019, *Nat. Astron.*, 3, 440
 Pierce J. C. S. et al., 2022, *MNRAS*, 510, 1163
 Pillepich A. et al., 2017a, *MNRAS*, 473, 4077
 Pillepich A. et al., 2017b, *MNRAS*, 475, 648
 Piotrowska J. M., Bluck A. F. L., Maiolino R., Peng Y., 2022, *MNRAS*, 512, 1052
 Planck Collaboration XVI 2014, *A&A*, 571, A16
 Planck Collaboration XIII 2016, *A&A*, 594, A13
 Pontzen A., Tremmel M., Roth N., Peiris H. V., Saintonge A., Volonteri M., Quinn T., Governato F., 2017, *MNRAS*, 465, 547
 Pracy M. B., Kuntschner H., Couch W. J., Blake C., Bekki K., Briggs F., 2009, *MNRAS*, 396, 1349
 Quai S., Pozzetti L., Citro A., Moresco M., Cimatti A., 2018, *MNRAS*, 478, 3335
 Quai S., Pozzetti L., Moresco M., Citro A., Cimatti A., Brinchmann J., Gunawardhana M. L. P., Paalvast M., 2019, *MNRAS*, 490, 2347
 Quai S., Hani M. H., Ellison S. L., Patton D. R., Woo J., 2021, *MNRAS*, 504, 1888
 Rodriguez-Gomez V. et al., 2015, *MNRAS*, 449, 49
 Rodríguez Montero F., Davé R., Wild V., Anglés-Alcázar D., Narayanan D., 2019, *MNRAS*, 490, 2139
 Roos N., Norman C. A., 1979, *A&A*, 76, 75
 Rosas-Guevara Y. M. et al., 2015, *MNRAS*, 454, 1038
 Rosas-Guevara Y., Bower R. G., Schaye J., McAlpine S., Dalla Vecchia C., Frenk C. S., Schaller M., Theuns T., 2016, *MNRAS*, 462, 190
 Roth N., Pontzen A., Peiris H. V., 2016, *MNRAS*, 455, 974
 Sanchez N. N., Tremmel M., Werk J. K., Pontzen A., Christensen C., Quinn T., Loeblman S., Cruz A., 2021, *ApJ*, 911, 116
 Satyapal S., Ellison S. L., McAlpine W., Hickox R. C., Patton D. R., Mendel J. T., 2014, *MNRAS*, 441, 1297
 Sazonova E. et al., 2021, *ApJ*, 919, 134
 Schawinski K., Urry M., Treister E., Simmons B., Natarajan P., Glikman E., 2011, *ApJ*, 743, L37
 Schaye J., Dalla Vecchia C., 2008, *MNRAS*, 383, 1210
 Schaye J. et al., 2015, *MNRAS*, 446, 521
 Setton D. J. et al., 2022, *ApJ*, 931, 51
 Shah E. A. et al., 2020, *ApJ*, 904, 107
 Silk J., Rees M. J., 1998, *A&A*, 331, L1
 Somerville R. S., Davé R., 2015, *ARA&A*, 53, 51
 Somerville R. S., Hopkins P. F., Cox T. J., Robertson B. E., Hernquist L., 2008, *MNRAS*, 391, 481
 Sparre M., Springel V., 2016, *MNRAS*, 462, 2418
 Sparre M. et al., 2015, *MNRAS*, 447, 3548
 Springel V., 2005, *MNRAS*, 364, 1105
 Springel V., 2010, *MNRAS*, 401, 791
 Springel V., Hernquist L., 2003, *MNRAS*, 339, 289
 Springel V., Di Matteo T., Hernquist L., 2005a, *MNRAS*, 361, 776
 Springel V. et al., 2005b, *Nature*, 435, 629
 Springel V., Di Matteo T., Hernquist L., 2005c, *ApJ*, 620, L79
 Springel V. et al., 2017, *MNRAS*, 475, 676
 Steinborn L. K., Hirschmann M., Dolag K., Shankar F., Juneau S., Krumpe M., Remus R.-S., Teklu A. F., 2018, *MNRAS*, 481, 341
 Terrazas B. A., Bell E. F., Henriques B. M. B., White S. D. M., Cattaneo A., Woo J., 2016, *ApJ*, 830, L12
 Terrazas B. A., Bell E. F., Woo J., Henriques B. M. B., 2017, *ApJ*, 844, 170
 Terrazas B. A. et al., 2020, *MNRAS*, 493, 1888
 Thorp M. D., Ellison S. L., Simard L., Sánchez S. F., Antonio B., 2019, *MNRAS*, 482, L55
 Toomre A., Toomre J., 1972, *ApJ*, 178, 623
 Torrey P., Cox T. J., Kewley L., Hernquist L., 2012, *ApJ*, 746, 108
 Trayford J. W. et al., 2017, *MNRAS*, 470, 771
 Villforth C. et al., 2014, *MNRAS*, 439, 3342
 Villumsen J. V., 1982, *MNRAS*, 199, 493
 Vogelsberger M., Genel S., Sijacki D., Torrey P., Springel V., Hernquist L., 2013, *MNRAS*, 436, 3031
 Vogelsberger M. et al., 2014, *MNRAS*, 444, 1518
 Weinberger R. et al., 2017, *MNRAS*, 465, 3291
 Weinberger R. et al., 2018, *MNRAS*, 479, 4056
 White S. D. M., 1978, *MNRAS*, 184, 185
 Wild V., Kauffmann G., Heckman T., Charlot S., Lemson G., Brinchmann J., Reichard T., Pasquali A., 2007, *MNRAS*, 381, 543
 Wild V., Walcher C. J., Johansson P. H., Tresse L., Charlot S., Pollo A., Le Fèvre O., de Ravel L., 2009, *MNRAS*, 395, 144
 Wild V., Heckman T., Charlot S., 2010, *MNRAS*, 405, 933
 Wild V. et al., 2020, *MNRAS*, 494, 529

Wilkinson S., Ellison S. L., Bottrell C., Bickley R. W., Stephen G., Jean-Charles C., Vivienne W., 2022, *MNRAS*, 516, 4354
Yang Y., Zabludoff A. I., Zaritsky D., Mihos J. C., 2008, *ApJ*, 688, 945
Zabludoff A. I., Zaritsky D., Lin H., Tucker D., Hashimoto Y., Shectman S. A., Oemler A., Kirshner R. P., 1996, *ApJ*, 466, 104
Zeng G., Wang L., Gao L., 2021, *MNRAS*, 507, 3301

Zheng Y., Wild V., Lahén N., Johansson P. H., Law D., Weaver J. R., Jimenez N., 2020, *MNRAS*, 498, 1259
Zinger E. et al., 2020, *MNRAS*, 499, 768

This paper has been typeset from a $\text{\TeX}/\text{\LaTeX}$ file prepared by the author.